Effect of waves on the leading-edge undulated tidal turbines

Weichao Shi [1 *], Mehmet Atlar[1], Rosemary Norman[2], Sandy Day[1], Batuhan Aktas[1]

1 Department of Naval Architecture, Ocean & Marine Engineering, University of Strathclyde, UK

2 School of Marine Science and Technology, Newcastle University, UK

Corresponding Author

Weichao Shi, Weichao.shi@strath.ac.uk

Department of Naval Architecture, Ocean & Marine Engineering,

Strathclyde University

Henry Dyer Building, 100 Montrose Street,

Glasgow G4 0LZ, U.K.

Tel: 0141 548 3237

Abstract: This paper presents an investigation on the efficiency performance of the leading-edge undulated tidal turbine blades under the effect of waves. This biomimetic blade application is inspired by humpback whale flippers which provide these mammals with an exceptional manoeuvring ability that is mainly accredited to the beneficial of their leading-edge tubercles. The paper first presents the design, optimisation and experimental validation of these turbine models. With the aim of further validating the efficiency performance in a different testing environment as well as exploring the combined effect of the tidal current and wave interaction, a test campaign in a towing tank facility was conducted. Both regular and irregular wave conditions were considered combining with varying towing speeds to simulate the tidal current effect. The test results revealed that the leading-edge undulated turbine has a stable hydrodynamic performance over a combined range of current speeds and waves indicating that the overall performance was not affected considerably by the combined effects as opposed to the performance solely due to steady tidal current.

Keywords: Wave-current interaction, Tidal turbine, Blade design, Leading-edge Tubercles, Biomimetic

1 Introduction

Humpback whale, known as one of the giant marine mammal species, is surprisingly agile while preying. This is mostly accredited to its highly efficient pectoral fins which are not smooth or streamlined as generally expected on performance swimmers. On the contrary, they are rough surfaces with undulated leading edges (Fish and Battle, 1996, Fish et al., 2011), which have drawn attentions of researchers and designers. The undulated leading edge is formed by the tubercles on the pectoral fins. This feature, which induces beneficial and chordwise counter-rotating vortices between the tubercles, provides the pectoral fins with an efficient performance in terms of delaying stall and improving the lift-to-drag ratio. These performance benefits were demonstrated through relatively recent wind tunnel tests for a pair of replica humpback whale flippers with and without leading-edge tubercles (Miklosovic et al., 2007, Miklosovic et al., 2004). Following this, investigations both numerical and experimental in nature, have looked at potential applications of leading-edge tubercles applied to air fans, wind turbines, rudders, propellers and so on (Ibrahim and New, 2015, Bolzon et al., 2016, Weber et al., 2010, Stanway, 2008, Howle, 2009, Corsini et al., 2013). However most of the research has focused on the foil performance under steady conditions, while rare studies have been conducted to investigate the performance in the unsteady conditions.

Recently a study has been conducted to explore the feasibility of applying this feature onto a tidal turbine blades (Shi et al., 2016a, Shi et al., 2016c, Shi et al., 2016b). This study first focused on the design and optimisation of the leading edge tubercles for a specific tidal turbine blade section by using numerical methods to propose an “optimum” design for the blade section. This optimum design was then applied onto a representative tidal turbine blade. This representative 3D blade demonstrated significant benefits especially after stall. The experimental measurements were further validated and complimented by numerical simulations using commercial CFD software for the detailed flow analysis.

Following that, a set of tidal turbine models with different leading-edge profiles was manufactured and series of model test campaigns were conducted in a cavitation tunnel to evaluate their efficiency, cavitation, underwater noise, and detailed flow characteristics. Based on these experimental investigations it was confirmed that the leading edge tubercles can improve: the hydrodynamic performance in the low Tip Speed Ratio (TSR, as defined in Equation 2) region without lowering the maximum power coefficient (Cp, as defined in Equation 3) (Shi et al., 2016c); constrain the cavitation development to within the troughs of the tubercles (Shi et al., 2016b); and hence mitigating the underwater noise levels (Shi et al., 2016b).

However, due to the complexity of natural environment, tidal turbines are operating not only in currents but also under the combined effect of waves. Therefore the performance of these leading-edge tubercles on the undulated turbine blades are questioned in the real sea conditions. To answer this question, this paper presents and discusses the results of a series of test campaigns with the leading-edge undulated turbine models in a controlled environment to evaluate their performances under the real sea conditions. The tests were conducted in the Kelvin Hydrodynamic Lab (KHL), Strathclyde University, under both regular waves and irregular waves. The efficiency and the thrust performances of the three model

turbines were investigated under the combined effect of the steady current and waves and findings were presented and discussed.

2 Description of the tested model

The biomimetic tidal turbine blade with an undulated leading edge was designed through the recent postgraduate study of the principle author (Shi, 2017). First, a reference turbine blade was chosen based on a previous research project in which a tidal turbine model was designed, tested and numerically modelled (Wang et al., 2007, Shi et al., 2013). The blade section of the reference turbine used the NREL S814 foil section, as shown in Figure 1. The main particulars and the definition of the main particulars for this 400mm diameter model turbine are shown in Table 1 and Figure 2 and based on this model, the leading-edge tubercles were applied to the blades.

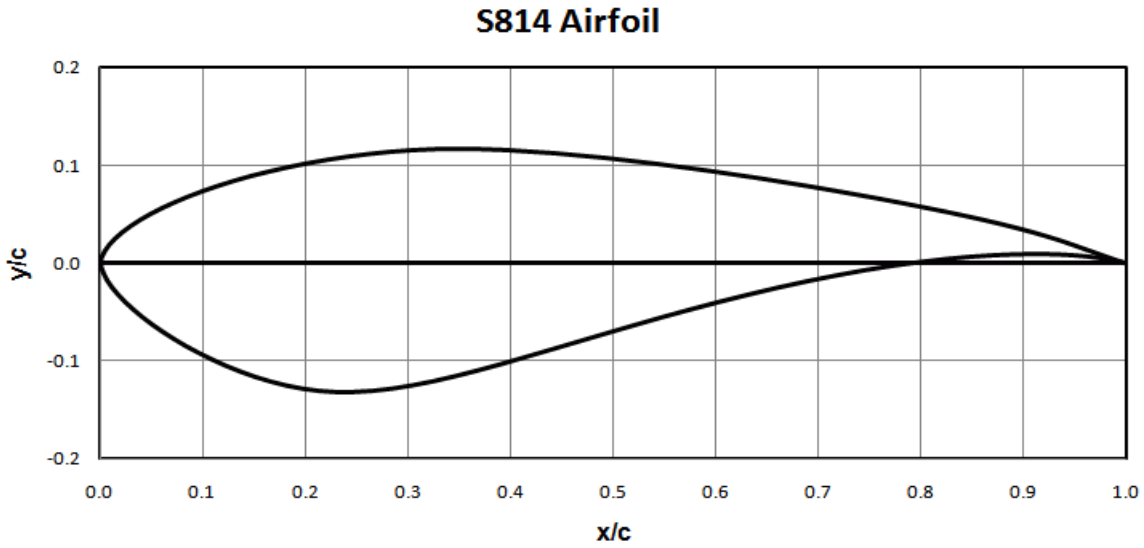

Figure 1. S814 foil section

Table 1. Main particulars of tidal stream turbine model

r/R	0.2	0.3	0.4	0.5	0.6	0.7	0.8	0.9	1
Chord length(mm)	64.35	60.06	55.76	51.47	47.18	42.88	38.59	34.29	30
Pitch angle (deg)	27	15	7.5	4	2	0.5	-0.4	-1.3	-2
Hub radius (0.2r) = 40mm; Same section profile, S814, along the radial direction									

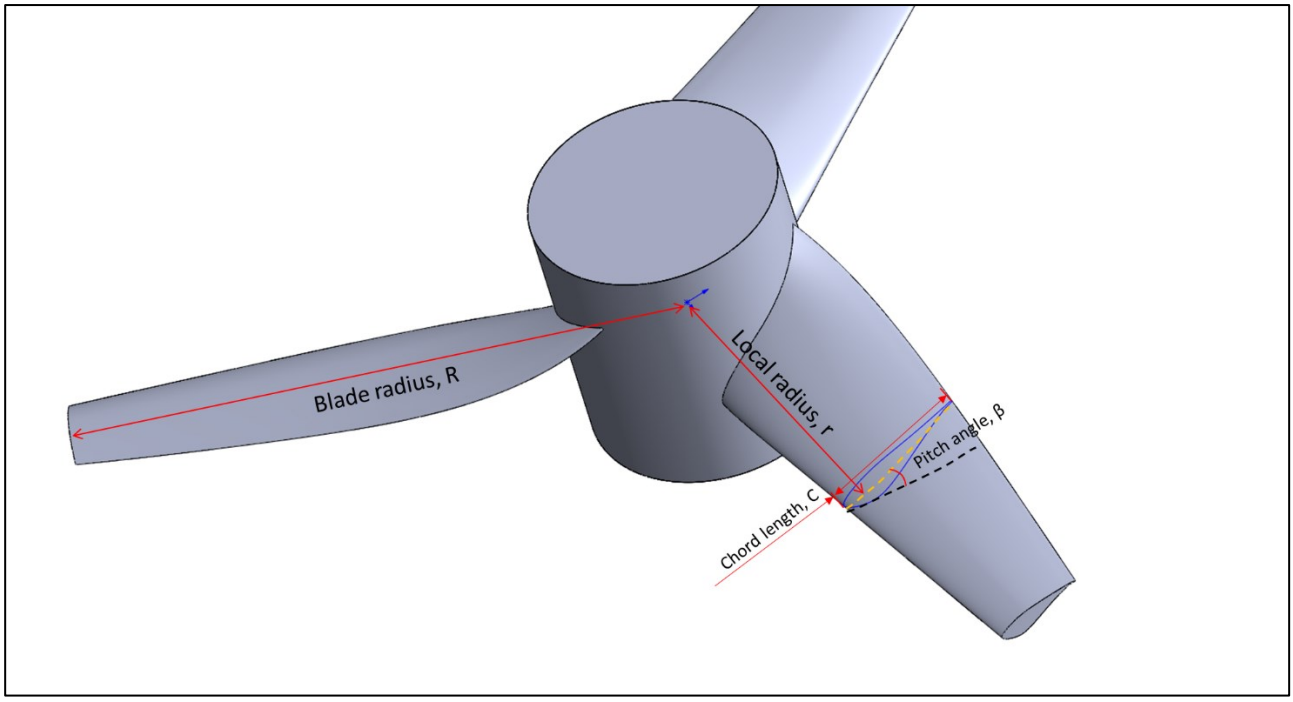

Figure 2 Definition of turbine blade geometry

2.1 Design and optimisation of tubercles for blade section, S814

After the reference turbine was chosen, a numerical optimisation study was carried out to design and optimise of the leading-edge tubercles for a thick and highly cambered blade section with the well-known S814 section profile. The sinusoidal form of tubercles was selected as the basis shape to conduct the numerical optimisation process. The investigation into the optimisation of the tubercle profiles was initiated by systematically changing two variants: the Height (H); and the Wavelength (W), of these protrusions based on the sinusoidal form of their shapes. The definitions of these parameters are shown in Figure 3.

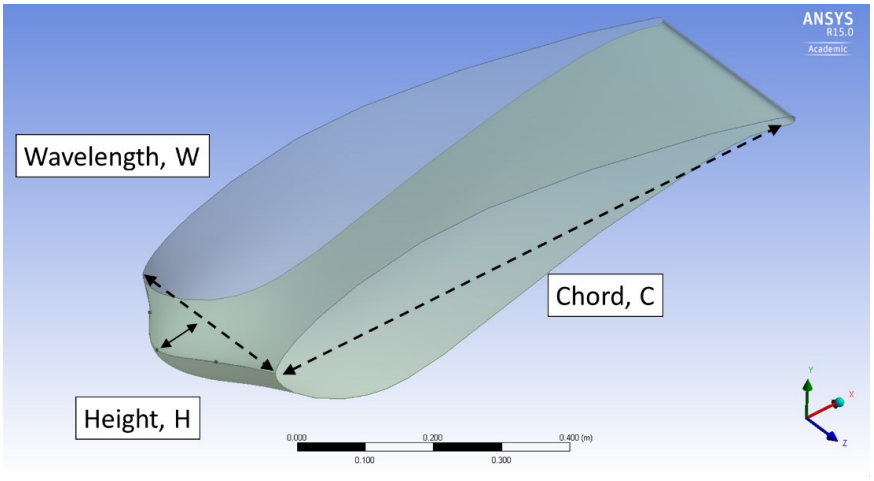

Figure 3 Definition of 2D foil with a sinusoidal tubercle

With the changing variants, the models were built, meshed and evaluated all in the integrated environment of ANSYS-Workbench which includes: ANSYS-Designmodeller as a geometry generator; ANSYS-Meshing as a mesh generator; and ANSYS-CFX as a CFD code for

performance evaluation. Based on the optimisation study for the 2D foil section, a sinusoidal form of leading-edge tubercle profile with *0.1C* height and *0.5C* wavelength appeared to be a good compromise for an optimum design as the maintained lift over the varied angles of attack (marked red in Figure 4) at a cost of slightly lowering the maximum lift coefficient, C_L (Shi et al., 2016a).

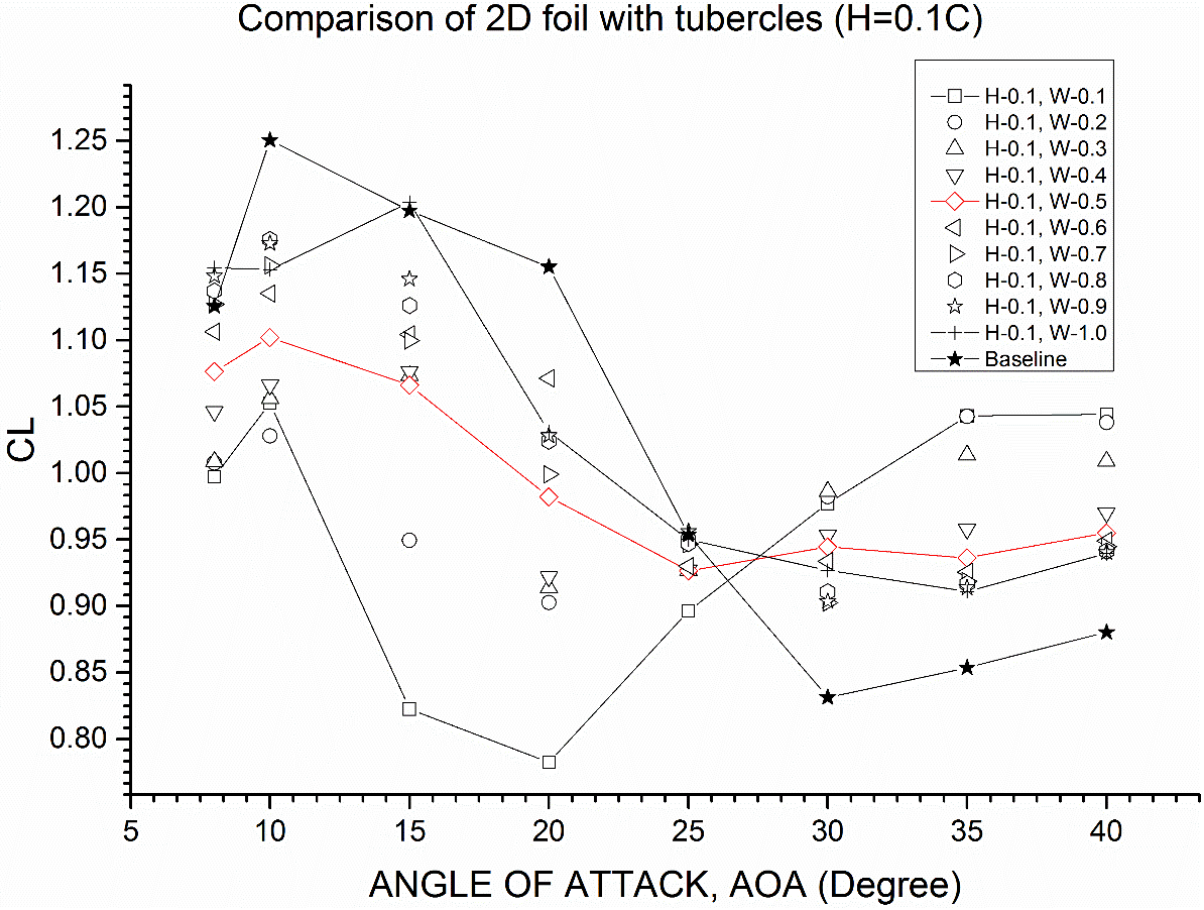

Figure 4 Comparison of 2D foil lift coefficients with different tubercle profiles by varying the wavelength (W) at constant tubercle height (H=0.1C)

2.2 Experimental investigation of a hydrofoil for the best tubercle coverage

The designed tubercle profile of *0.1C* height and *0.5C* wavelength was applied onto a specially manufactured, carbon-fibre model hydrofoil with interchangeable leading-edge profiles. This hydrofoil is a straightened turbine blade with the same chord length distribution but a constant pitch angle, of which the leading edge is modularized and 3D printed. In total 4 interchangeable modules with smooth leading edge and 4 modules with tubercles were prepared to test various combinations of the leading-edge profiles with changing the tubercle coverage as shown in Figure 5.

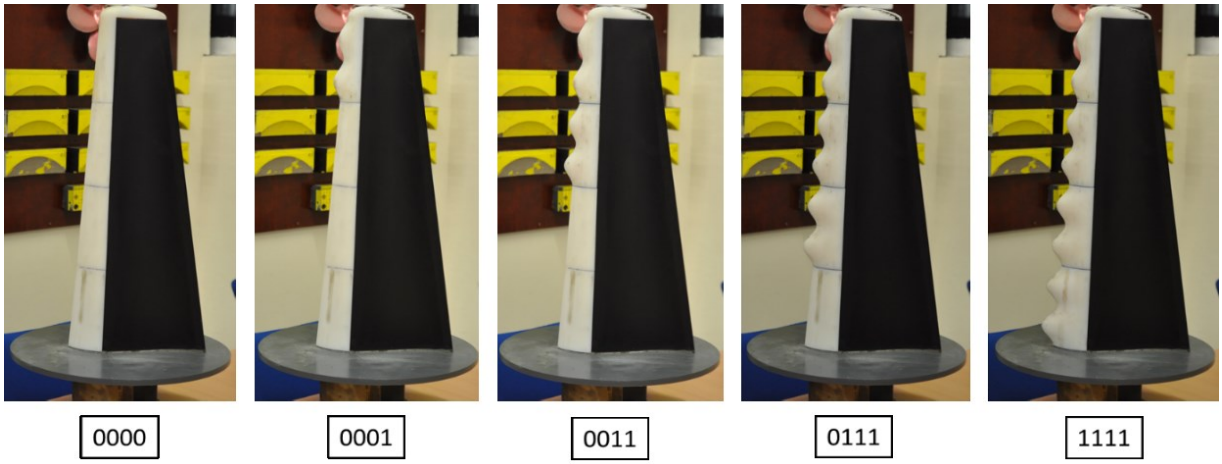

Figure 5 Tested 3D hydrofoil models with interchangeable leading-edge parts

Based on the measurements of the lift and drag characteristics of the different tubercle arrangements, the comparisons of the lift-to-drag ratios appear that Foil "0001", which had 1/4 of its leading-edge covered with tubercles, displayed an overall better performance. This can be clearly seen in Figure 6 where Foil "0001" shows a positive impact from 0° to 26° of angle of attack (AOA) with more than 10% enhancement in the maximum lift-to-drag ratio at 5° of AOA, compared to the reference (Foil "0000"). Even though Foil "1111" displayed the highest growth rate at 16° AOA, Foil "0001" may offer more potential in improving the performance of a tidal turbine operating over a wider range of tip speed ratios. This experimental study is documented within more details in (Shi et al., 2016a).

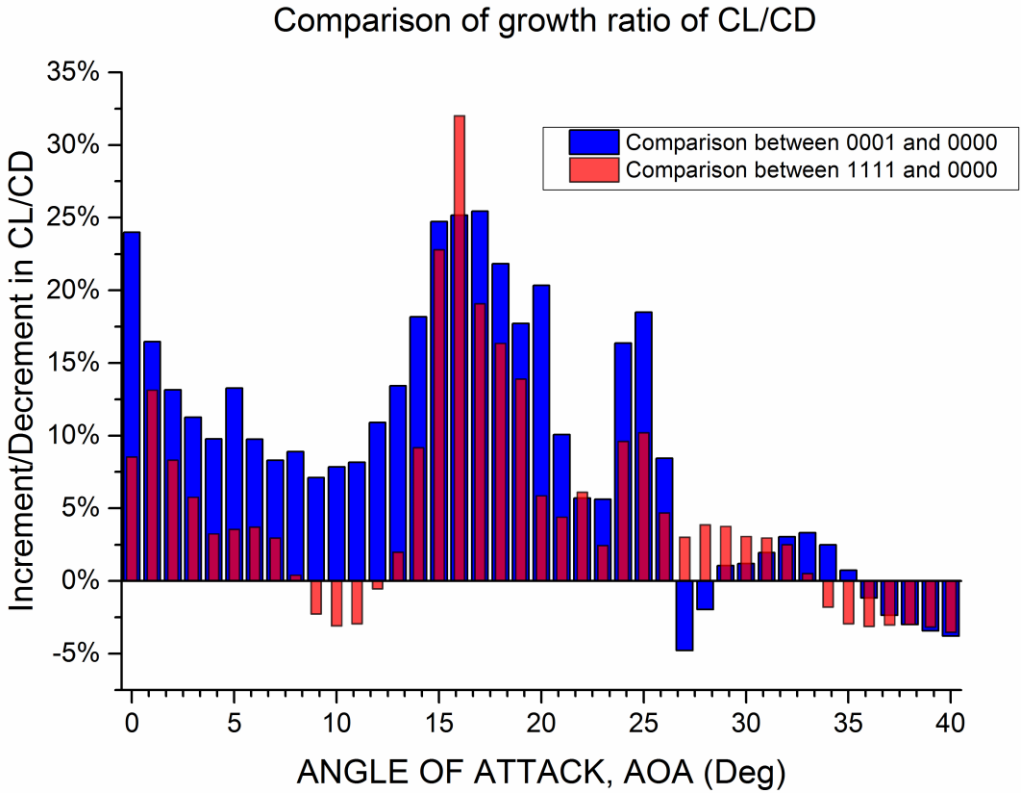

Figure 6 Comparison of relative growth ratios for C_L/C_D for Foil "1111" (with leading-edge tubercles applied on whole span) and Foil "0001" (with minimum leading-edge tubercles applied around the tip)

2.3 *Cavitation tunnel tests for the performance evaluation*

Three pitch-adjustable turbine models with different leading-edge profiles were manufactured from bronze material by Centrum Techniki Okrętowej S.A. (CTO, Gdansk), as shown in Figure 7. "Ref" refers to the turbine model with a smooth leading edge; while "Sin2" refers to the one with two leading-edge tubercles at the tip which performed most efficiently in the hydrofoil tests; and the one with eight leading-edge tubercles is named "Sin8" which presented the maximum lift coefficient as well as the most sustained linear increase of the lift during the hydrofoil test. The sinusoidal leading-edge profile was developed as shown in Figure 8. The amplitude (A) of the sinusoidal tubercles was equal to 10% of the local chord length (C) while eight tubercles were evenly distributed along the radius with the wavelength (W) equal to 20mm. The profile of the leading tubercles was as represented by Equation 1.

$$H = \frac{A}{2} cos\left[\frac{2\pi}{W}(r - 40) - \pi\right] + \frac{A}{2} \qquad \text{Equation 1}$$

where H is the height of the leading-edge profile relative to the reference one which has the smooth leading-edge profile.

Figure 7. Tested turbine models

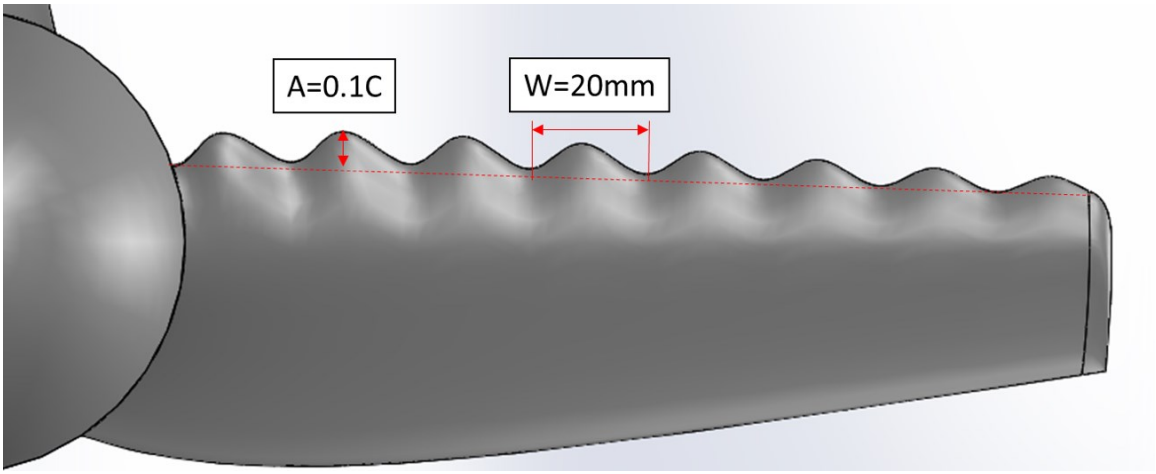

Figure 8. 3D design of the turbine blade with leading-edge tubercles

Before the wave-current interaction tests, which is the main objective of this paper, these three turbine models were tested in the Emerson Cavitation Tunnel of Newcastle University. These tests showed significant improvement in the turbine performance in terms of improving its power coefficients *(C_P)* in lower TSRs without compromising the maximum,

value of C_P, limiting the cavitation development and lowering the underwater radiated noise level (Shi et al., 2016c, Shi et al., 2016b).

The hydrodynamic test result under 2m/s incoming velocity was presented in Figure 9. In this figure, the pitch angle setting was increased to +4° which was the most efficient pitch angle setting for the reference turbine. The leading-edge tubercles can contribute more torque as represented by the power coefficient *(Cp)* at the lower end of the TSR range as well as thrust as represented by the thrust coefficient *(Ct/10).* A maximum of 30% more torque can be produced at TSR=1.5. Compared with Sin_2, the impact caused by Sin_8 is more obvious in both *Cp* and *Ct/10*. The leading-edge tubercles did not have any effect on the maximum *Cp* apart from shifting its TSR from 3.5 to 4.0. The effect of tubercle is similar under varied pitch angles and Reynolds numbers.

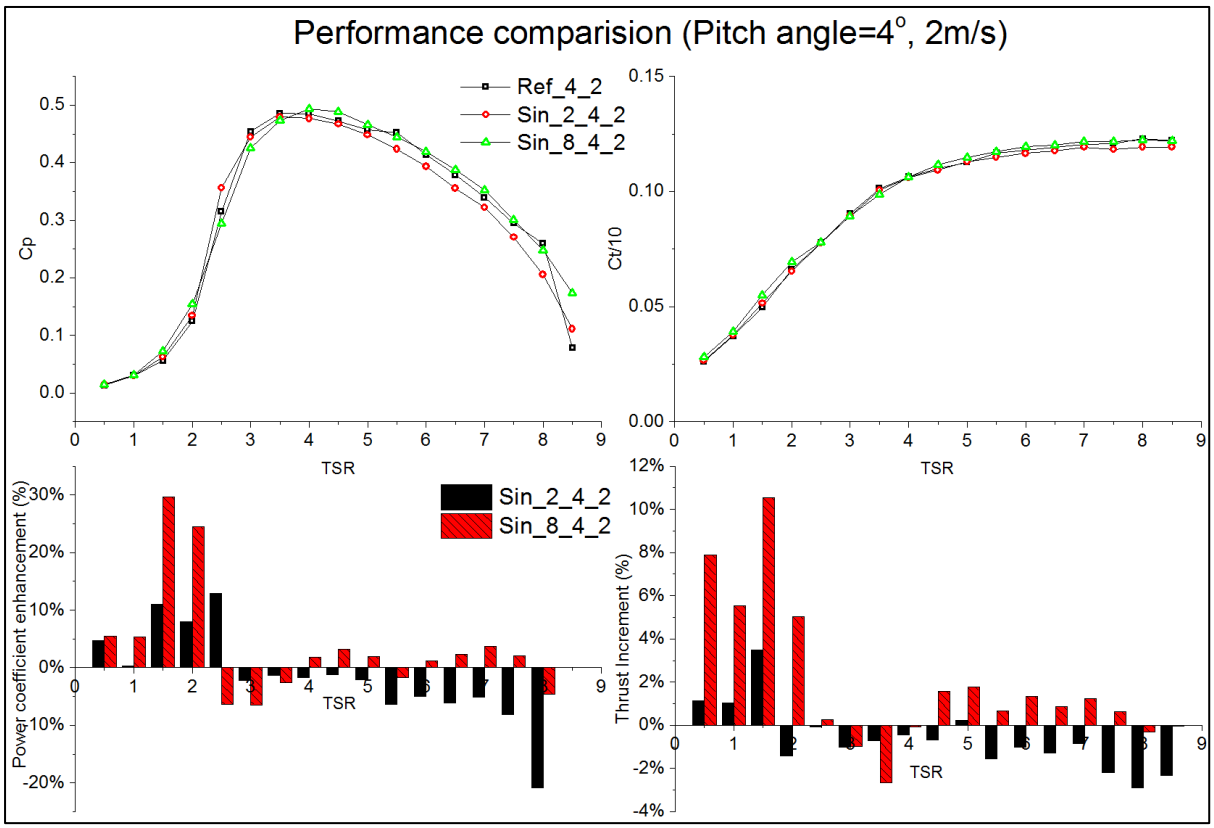

Figure 9 Experimental result of model turbine performance in a cavitation tunnel (Pitch=4°, 2m/s)

Following the experimental campaign in the cavitation tunnel, the following experimental investigation in a towing tank was planned to further validate the performance of these biomimetic turbines and to explore the combined wave-current effect on the turbine performance.

3 Experimental setup and approach

3.1 Description of the Kelvin Hydrodynamic Lab

The experiments were conducted in the Kelvin Hydrodynamic Lab (KHL), Strathclyde University by using its towing tank facility which is 76m in length, 4.6m in width and 2.5m in depth. As shown in Figure 10, one end of the tank is equipped with a variable-water-depth, computer-controlled four-flap absorbing wave-maker generating regular or irregular waves over 0.5m height while the opposite end is fitted with a high-quality variable-water-depth sloping beach, with reflection coefficient typically less than 5% over frequency range of interest.

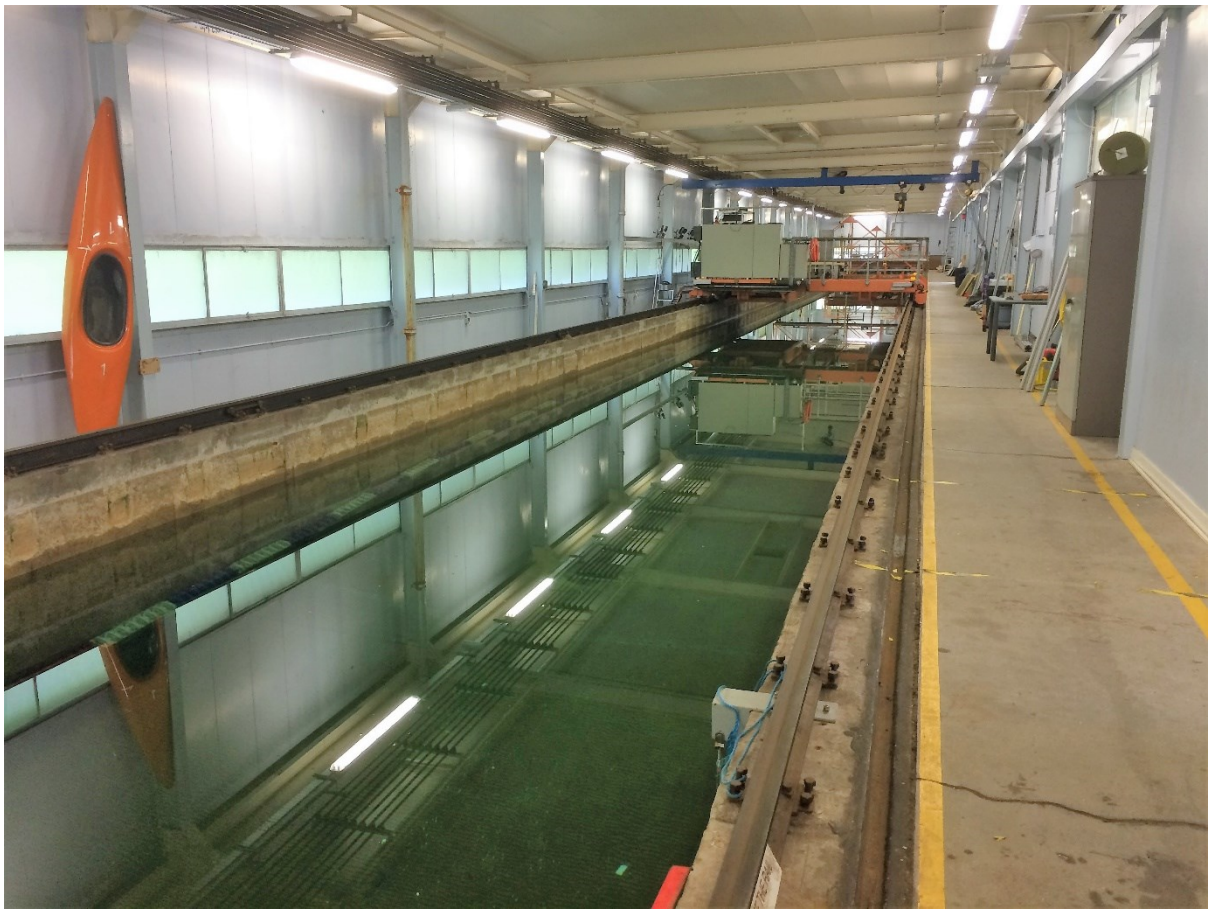

Figure 10 KHL towing tank

3.2 Experimental setup

The towing tank of KHL is equipped with the self-propelled Kempf & Remmers towing carriage with a max speed of 5m/s on which an open water dynamometer can be attached to drive the turbine models. The open water dynamometer, that KHL is using, is an in-house built dynamometer driven by a 900w AC motor decelerated by a 10:1 gear box, which has a maximum 300 RPM, specially designed for tidal turbine testing. To get rid of the electrical noise, the cases of the motor and the whole body are connected to the earth. The torque and thrust are measured by a torque and thrust transducer with the capability to measure 2000N thrust and 50NM torque. The frictional torque of the system was also calibrated before the

test and corrected during the tested. All the signals and power supplies are all transferred through a multi-channel slip ring. A general view of the dynamometer and model fitting at the towing carriage can be seen in Figure 11. A sonic wave probe fitted onto the carriage was used to measure the height and the encounter frequency of the waves. All the measurement data was acquired at 137 Hz as the sample frequency.

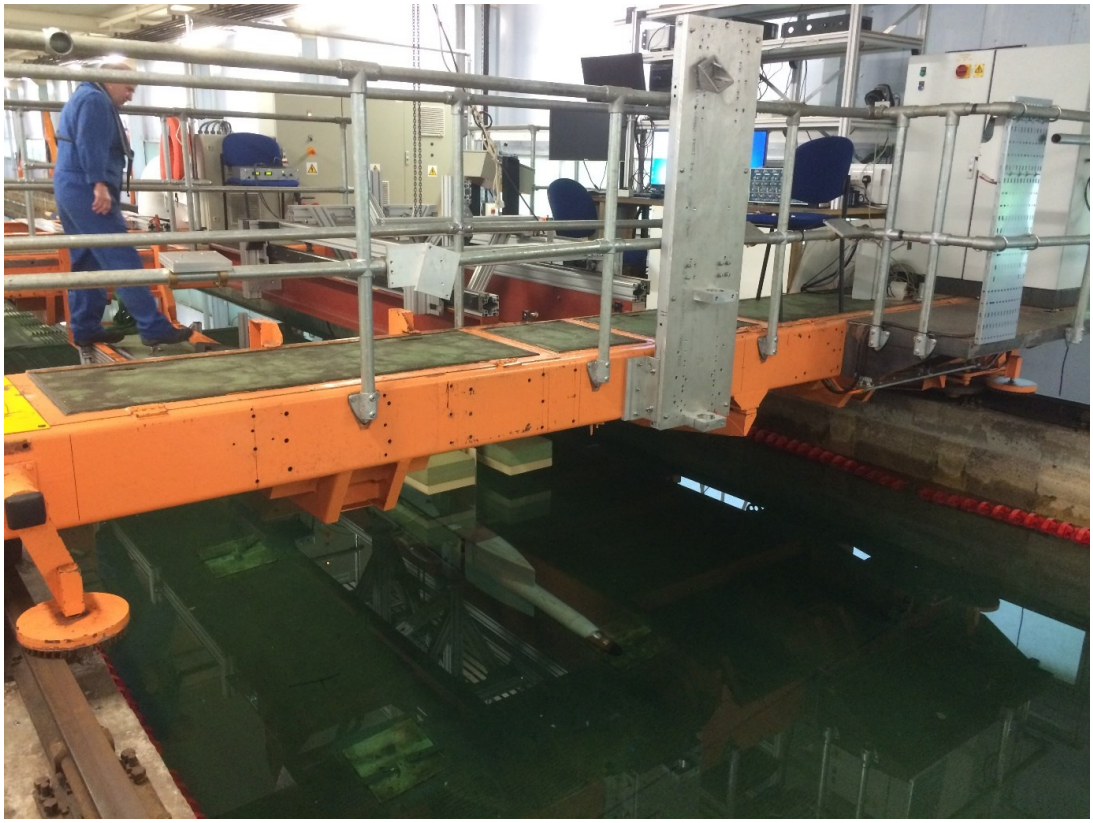

Figure 11 Turbine model and dynamometer fitting onto the towing carriage

The turbine was mounted on the dynamometer. The rotational speed is controlled by the motor to achieve the desired Tip Speed Ratio (TSR) which can be calculated using Equation 2. During the model tests, the torque and thrust of the turbine were measured and from these measurements the power coefficient (Cp) and the thrust coefficient (C_T) can be derived by using Equation 3 and Equation 4 respectively:

$$TSR = \frac{\omega r}{V} \quad \text{Equation 2}$$

$$Cp = \frac{Q\omega}{\frac{1}{2}\rho A_T V^3} \quad \text{Equation 3}$$

$$C_T = \frac{T}{\frac{1}{2}\rho A_T V^2} \quad \text{Equation 4}$$

where Q is the torque of the turbine, in Nm; T is the thrust, in N; ω is the rotational speed, in rad/s; A_T is the swept area of the turbine and equals $\pi D^2/4$, m^2; ρ is the tank water density, in kg/m^3; V is the incoming velocity, in m/s, D is the turbine diameter, in m.

As the performance of the turbine is strongly dependent on the Reynolds number, this non-dimensional numbers at 0.7 radius of the turbine blade, $Re_{0.7r}$ were monitored and can be derived from Equation 5.

$$Re_{0.7r} = \frac{C_{0.7r}\sqrt{(V^2 + (0.7\omega r)^2}}{\nu} \quad \text{Equation 5}$$

where $C_{0.7r}$is the chord length of the turbine at 0.7 radius, m; ν is the kinematic viscosity of the water, m^2/s.

The uncertainty level of the towing tank tests was well controlled with a 0.3% for the TSR, 1.1% for the Cp and 0.2% for Ct/10 which were based on 7 individual tests for TSR=4. In addition all the test runs were repeated twice for the repeatability checks.

3.3 Test matrix

The initial set of the tests with the three model turbines involved the open water performance measurements in steady current (i.e. calm water). The testing matrix in Table 2 is to investigate the effect of Reynolds number on the turbine performance, followed by the test matrix in Table 3 for the open water performance test in a range of TSRs with the highest achievable Reynolds number.

Table 2 Test matrix for Reynolds number test

TSR	RPM	V(m/s)	$Re_{0.7r}$
Reynolds number test			
4	50	0.262	29,317
4	100	0.524	58,634
4	150	0.785	87,950
4	200	1.047	117,267
4	250	1.309	146,584

Table 3 Test matrix for open water performance test

Open water performance test			
TSR	RPM	V(m/s)	$Re_{0.7r}$
1	150	3.142	144,433
2	250	2.618	169,643
2.5	250	2.094	158,993
3	250	1.745	152,897
3.5	250	1.496	149,101
4	250	1.309	146,584
5	250	1.047	143,568
6	250	0.873	141,903

The next two sets of the experiments involved the performance measurements with the same model turbines in waves: firstly in regular waves with two different wave amplitudes and over a range of frequencies as shown in Table 4; and secondly in irregular waves defined by three different JONSWAP wave spectra as shown in Table 5. Table 5 also indicated the corresponding full-scale conditions of the tested JONSWAP spectra for a 20m diameter turbine.

Table 4 Test matrix for regular wave test

Regular wave tests (Dia=0.4m, Shaft submergence=1.1m)					
TSR	N (RPM)	V (m/s)	Re	Wave Amplitude (m)	Wave Frequency (Hz)
4	250	1.309	146,584	0.05	0.3~0.9
4	250	1.309	146,584	0.1	0.3~0.9

Table 5 Test matrix for irregular wave test and corresponding full-scale conditions

Irregular wave tests (Dia=0.4m, Shaft submergence=1.1m)							
Sea State	TSR	N (RPM)	V (m/s)	Re	JONSWAP, Hs (m)	JONSWAP, Tp (s)	
NO.1	4	150	0.785	87,950	0.15	1.581	
NO.2	4	150	0.785	87,950	0.25	2.214	
NO.3	4	150	0.785	87,950	0.3125	2.372	
Full-scale (corresponding) conditions of Irregular wave test (Dia=20m, Shaft submergence=55m)							
Sea State	TSR	N (RPM)	V (m/s)	Re	JONSWAP, Hs (m)	JONSWAP, Tp (s)	Return period
NO.1	4	21.01	5.50	3.08E+07	7.5	11.18	1 year
NO.2	4	21.01	5.50	3.08E+07	12.5	15.65	10 year
NO.3	4	21.01	5.50	3.08E+07	15.625	16.77	100 year

During the irregular wave tests, 250 wave encounters were guaranteed by multiple runs depending on the test conditions. Two turbines were tested which were the reference turbine (Ref) and biomimetic turbine with full tubercles (Sin8). Modelling of the irregular waves was carried out based on the specified significant wave height H_s, peak wave period T_p and spectral peakedness parameter γ=3.3 in the JONSWAP spectrum given by Equation 6. The three tested JONSWAP spectra were plotted as shown in Figure 12.

$$S(f) = \alpha H_s^2 T_p^{-4} f^{-5} \exp\left[-1.25\left(T_p f\right)^{-4}\right] \gamma^{\exp\left[-\left(T_p f - 1\right)^2 / 2\sigma^2\right]} \qquad \text{Equation 6}$$

where, $S(f)$ is the spectral wave energy density distribution; f is the wave frequency (Hz); f_p is the peak wave frequency (Hz), 1 / *Tp*; σ = 0.09 for $f > f_p$ and σ =0.07 for $f < f_p$; and

$$\alpha = \frac{0.0624}{0.230 + 0.0336\gamma - 0.185/(1.9+\gamma)}.$$

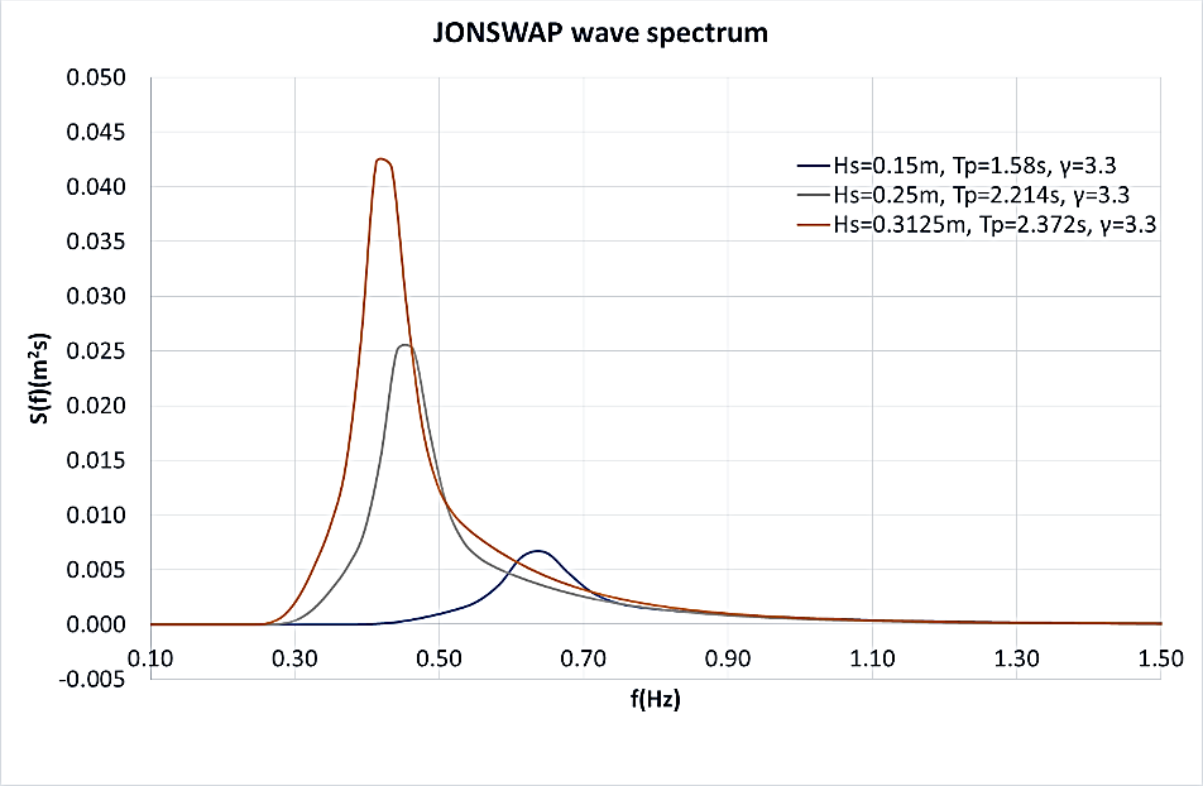

248

249 Figure 12 JONSWAP wave spectra generated in model tests

250

4 Results and discussions

4.1 Reynolds number effect

In order to analyse the effect of the Reynolds number, the three turbines were tested with five different Reynolds numbers at the TSR = 4. Based on the measured torque and thrust the analysed Cp and Ct/10 are presented in Figure 13. As shown in this figure the values of Cp and Ct/10 rise up with the increasing Re. However, these coefficients for the turbines with tubercles, “Sin2” and “Sin8”, are less sensitive to the change in Re number compared with the reference turbine, “Ref”, especially for Cp. This was potentially because of the waviness caused by the tubercles in the leading edge was tripping the laminar flow to move into the transition or turbulent regime.

Because of the limited Reynolds number, that can be reached in these tests, the maximum Re condition was used in the following performance tests. However, the Reynolds number effect still had to be born in mind even with the use of the max Re number. Having said that these tests clearly demonstrated more stable performance for the biomimetic turbine as such the power generation efficiency was not dependent on the incoming velocity. This effect is expected as the leading-edge undulation will excite the streamwise contra-rotating vortices which can energise the flow and accelerate the flow transition, as shown in Figure 14.

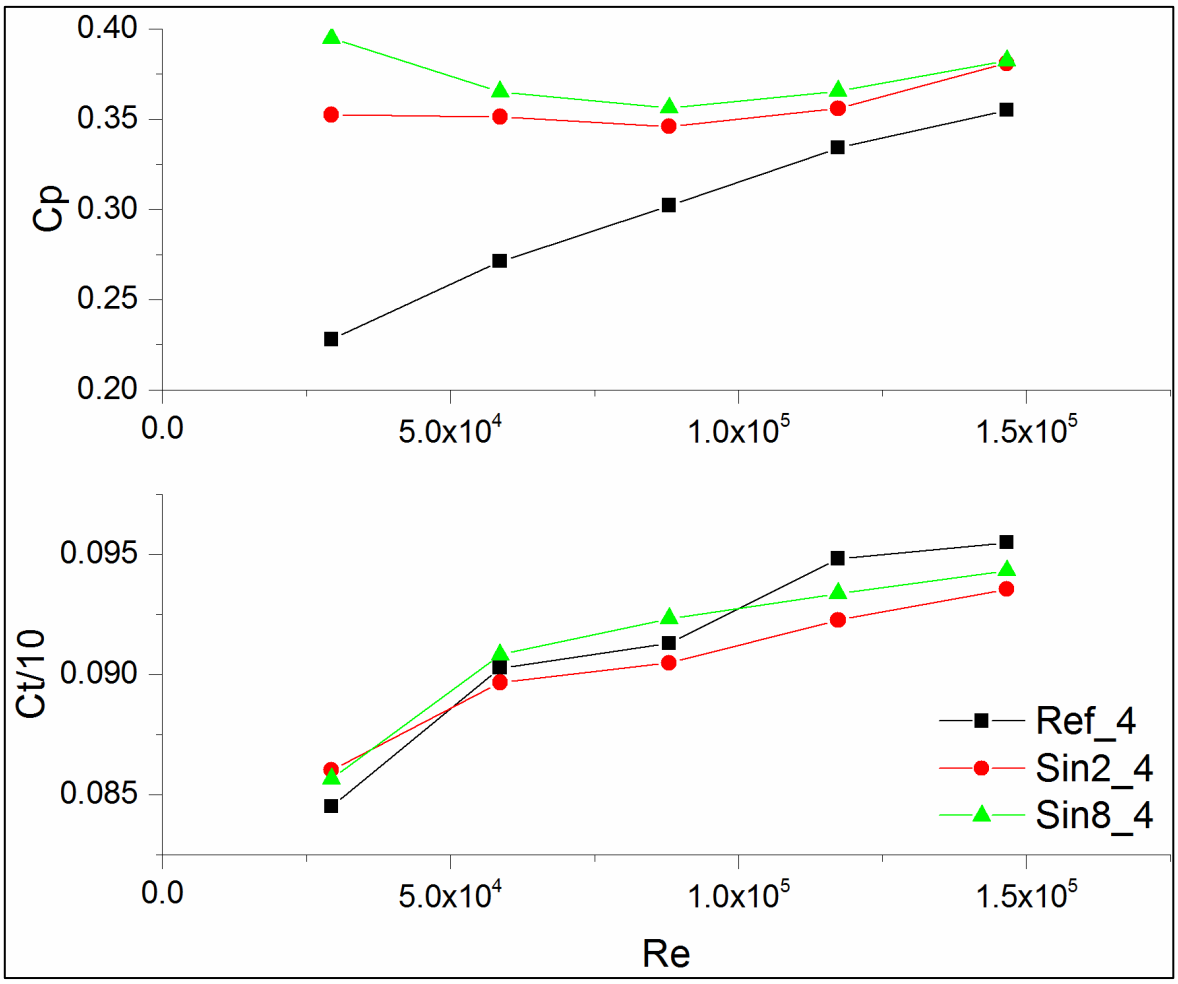

Figure 13 Results of Reynolds number effect test

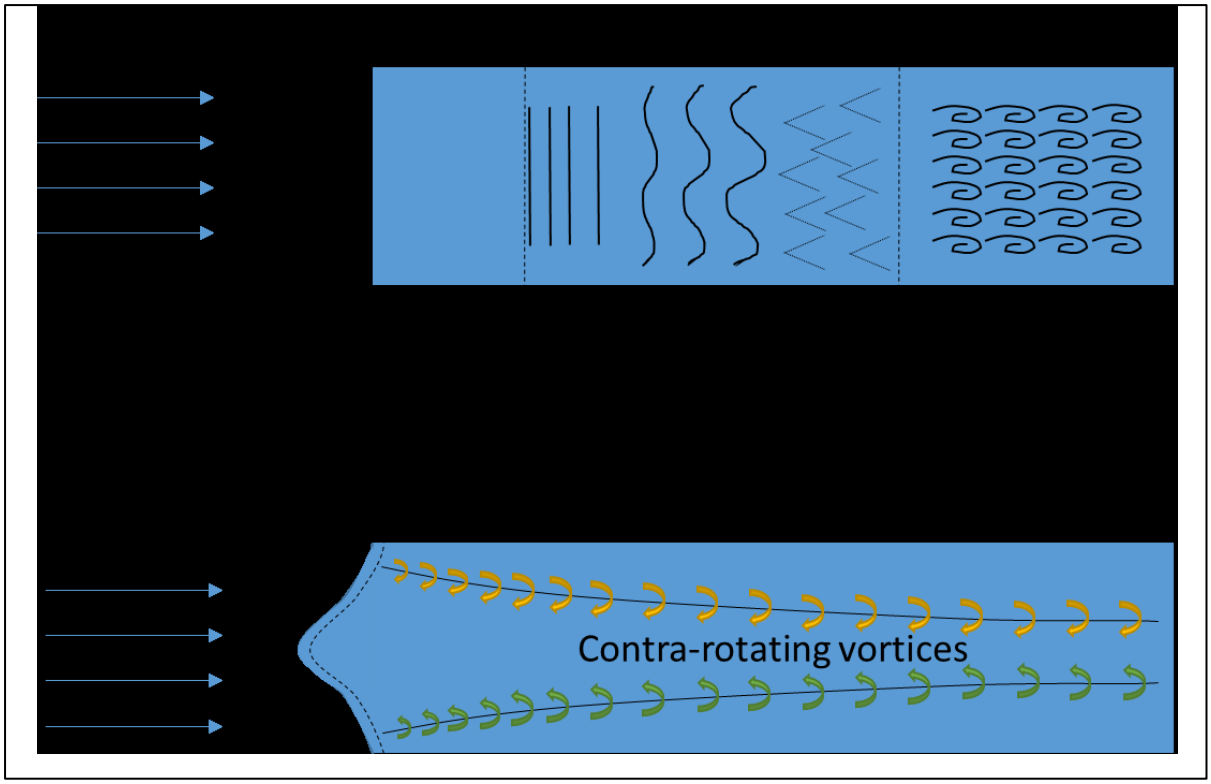

Figure 14 Schematic description showing a turbulence development on a conventional blade and the one on a leading-edge undulated blade

4.2 Open water performance tests in the towing tank

After the Reynolds number effect tests, open water performance tests with constant carriage speed were conducted for the three models to evaluate their hydrodynamic performance in the towing tank as it has been done in the cavitation tunnel. The test results are shown in Figure 15. Because of the limited Re number, the coefficients of Cp and Ct/10 have shown significantly lower performance. The maximum Cp of the reference turbine tested in the cavitation tunnel as shown in Figure 9 is around 48%, whereas the maximum Cp of the reference turbine in the towing tank is around 40%, which indicated 20% less. This might be not only because of the significant difference in the Reynolds numbers but also because of the difference in the blockage ratios between the two facilities. However, due to nature of the relative comparisons, only the performance results of the tests conducted in the towing tank were compared and discussed in the following.

As shown in Figure 15, even though the magnitudes of the results from these two facilities have shown certain level of disparity, the same trend in the effect of the tubercles on the results of the towing tank test based performances can be observed as such: the tubercles still improved the performance in the low TSR region without compromising the peak Cp; Sin8 showed the best performance with a slightly shifted Cp curve compared with the reference turbine; general performance of Sin2 was very close to the reference turbine but also with the improved performance in low TSRs.

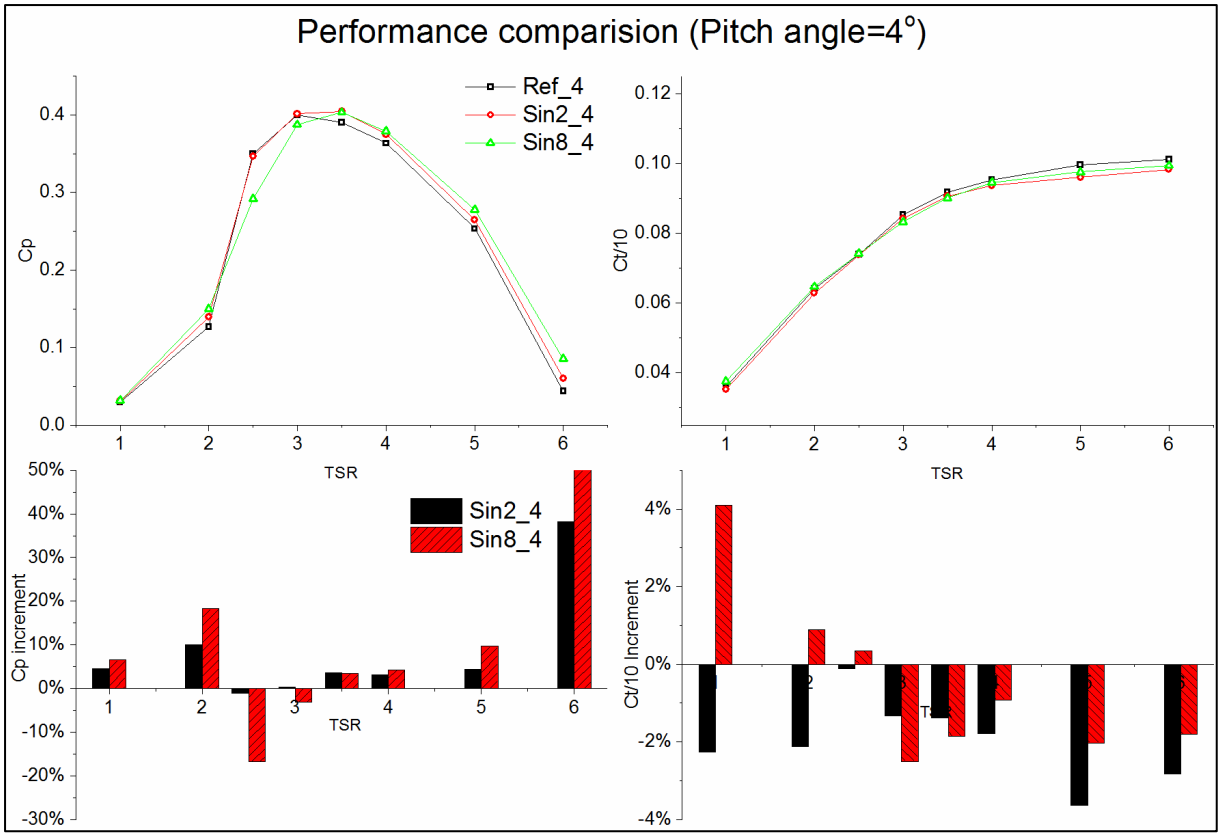

Figure 15 Test result of open water performance in the towing tank

4.3 *Wave-current interaction tests in regular waves*

Following the open water performance tests in calm water, the same tests were conducted in regular waves with two different wave amplitudes (0.05m and 0.1m) and over a range of incoming wave frequencies (0.3-0.9Hz). As shown in Table 4, all the regular wave tests were carried out for TSR=4, RPM=250 and V=1.309m/s. The time history of the wave height, torque and thrust of the turbines were recorded and then the peak amplitude Fast Fourier transfer analysis (FFT analysis) was applied using Hanning window function.

Typical results of time history records and FFT analyses of a sample test run are shown in Figure 16 where the regular wave with a distinct encounter frequency generated significant fluctuation on the torque and thrust records. One can also observe two further peaks in the torque and thrust around the 1st blade passing frequency (12.5Hz) and shaft rotating frequency (4.17Hz), which might be caused by the shaft friction and non-uniform incoming flow. However, these two peaks were very stable throughout the whole tests even with different wave frequencies. Therefore, in order to identify the fluctuation caused by the wave action, which may cause fatigue failure for the tidal turbine, the peaks of the torque and thrust at encounter wave frequencies were excluded in the analyses.

Uncertainty analysis for the wave test

The uncertainty levels were also checked by four times of repeat tests with the reference turbine for the test runs in waves with an amplitude of 0.1m and wave frequency of 0.5Hz. As

314 shown in Table 6, the results of the measurements for the torque and thrust at the same
315 encounter frequencies were quite repeatable with small values of standard deviations.

316 Table 6 Uncertainty analysis of the wave test

Real Carriage Speed (m/s)	Real TSR	Encounter Frequency (Hz)	Torque Fluctuation Amplitude (NM)	Thrust Fluctuation Amplitude (N)	Average Cp	Average Ct/10
1.30713	4.005728	0.69978	0.679986	17.160794	0.384556	0.97679
1.30729	4.005229	0.69978	0.674702	17.089281	0.385723	0.97423
1.3072	4.005507	0.69978	0.671198	17.147577	0.386217	0.977304
1.30712	4.005758	0.69978	0.675299	16.868419	0.387079	0.977287
Percentage of standard deviations (%)			0.53%	0.79%	0.27%	0.15%

317

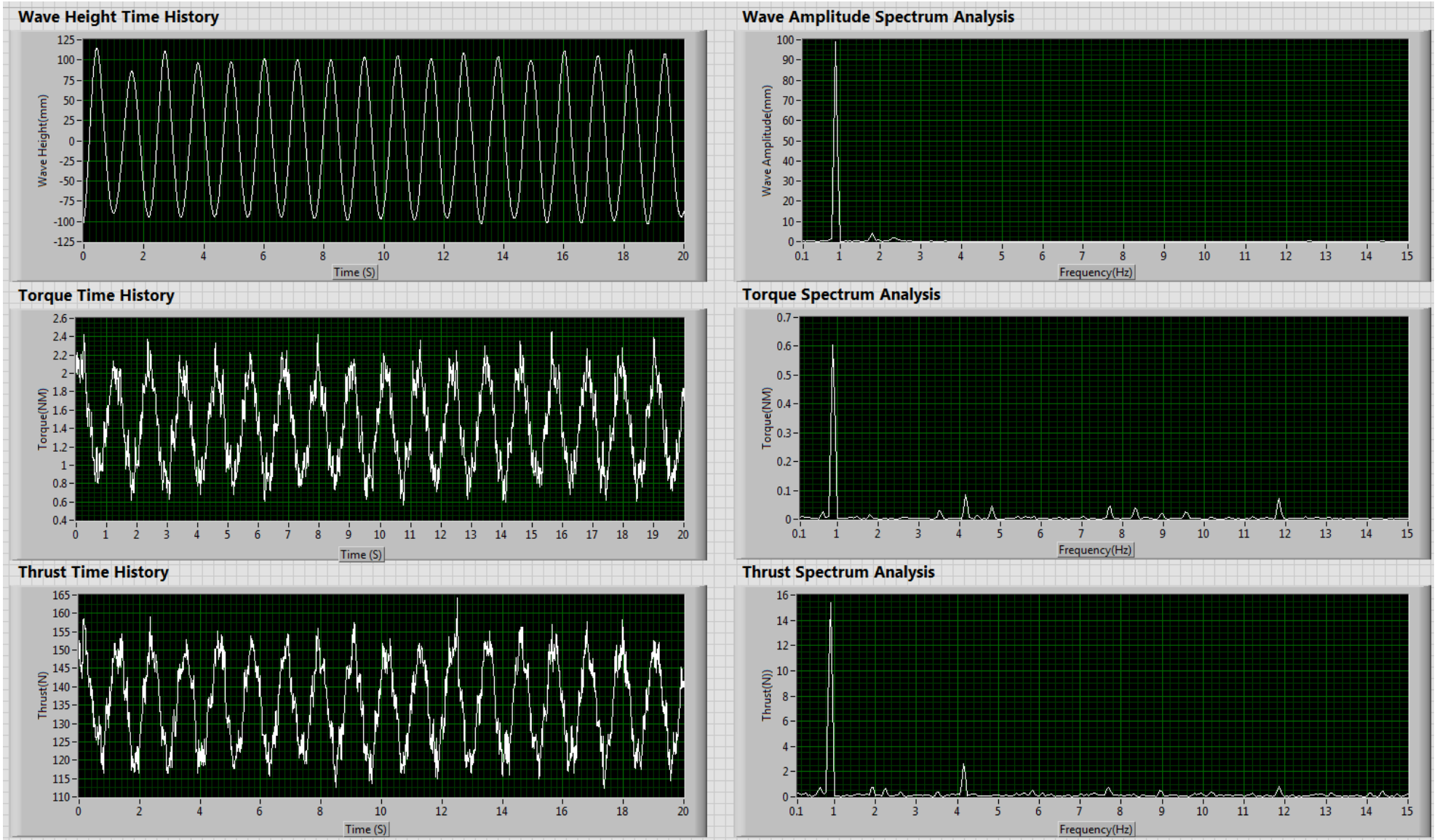

Figure 16 Time history and FFT analysis for the regular wave test

4.3.1 Effect of regular wave action on the performance of turbines

The analysed results of the time averaged power coefficient (Cp) and thrust coefficient (Ct/10) for each encounter frequency tested are presented in Table 7 and Table 8 the wave amplitude of 0.05m and 0.10m, respectively. These coefficients were normalized against the corresponding Cp and Ct/10 values in calm water for the same tip-speed ratio, TSR=4.

Table 7 Normalized time average Cp and Ct/10 in regular wave test at wave amplitude=0.05m and TSR=4

Encounter wave frequency	Normalized Averaged Ct/10			Normalized Averaged Cp		
(Hz)	Ref	Sin2	Sin8	Ref	Sin2	Sin8
1.54952	1.00260	0.99059	1.00012	0.99261	0.98216	0.99944
1.34957	1.00563	1.00025	1.00947	1.00231	0.99761	1.01657
1.09965	1.00854	1.00866	1.00910	1.00960	1.01437	1.02035
0.89971	1.01450	1.00971	1.01304	1.03353	1.02217	1.02716
0.69978	1.01718	1.01222	1.01078	1.04775	1.02091	1.01681
0.54982	1.01280	1.01074	1.00498	1.02144	1.02608	1.00144
0.39987	1.00794	1.00893	1.00205	1.01362	1.02345	1.00472
Calm water	1	1	1	1	1	1

Table 8 Normalized time average Cp and Ct/10 in regular wave test at wave amplitude=0.1m and TSR=4

Encounter wave frequency	Normalized Averaged Ct/10			Normalized Averaged Cp		
(Hz)	Ref	Sin2	Sin8	Ref	Sin2	Sin8
1.54923	0.99165	0.99783	1.00036	0.9819	0.99761	0.9982
1.29958	1.00666	1.00414	1.00280	1.00555	1.00891	1.00514
1.09965	1.01034	1.00614	1.00826	1.01625	1.01939	1.01617
0.89971	1.01810	1.01641	1.01559	1.03896	1.04049	1.03551
0.69978	1.02375	1.01515	1.01665	1.05632	1.04570	1.04519
0.54982	1.01436	1.01525	1.00778	1.04811	1.04999	1.03546
0.39987	1.01151	1.00677	1.00106	1.04986	1.04357	1.02837
Calm water	1	1	1	1	1	1

As can be seen in Table 7, the impact of the waves on the Ct/10 of all three turbines was very limited within 2%, while the impact on the Cp was slightly larger but still within 5%. Meanwhile, the reference turbine appeared to be relatively more sensitive to the wave action (by a max of 4.8% increase in Cp) while the ones with tubercles were less sensitive by a max of 2.6% increase in Cp for the Sin2 and 2.7% for the Sin8, respectively. This kind of performance enhancement could be because of the turbulent flow generated by the action of small waves.

Similar form of performance enhancement can be also observed with bigger waves, as shown in the Table 8. But the differences in performance change between the reference turbine and the turbine with tubercles got smaller: a maximum 5.6% Cp enhancement for the reference

turbine; while 5.0% and 4.5% for the Sin2 and the Sin8 respectively. The impact of the wave effect on the coefficient, Ct/10 was even smaller within 2.5% for all three turbines.

Based on the above result, it can be seen that the wave action on the performance of the turbine can be beneficial in terms of performance enhancement, but this kind of enhancement is limited within 5% depending on the wave condition.

4.3.2 Effect of regular wave action on the performance fluctuations of turbines

Apart from the impact on the averaged performance, the fluctuation on the torque and thrust can be a further concern on the performance of a tidal turbine. The fluctuation in torque is concern for the quality of the generated power while the fluctuation in thrust is concern for the supporting structure. In order to shed a light on this aspect Table 9 and Table 10 are included.

In these tables, Table 9 and Table 10, the percentage of Cp and Ct/10 fluctuation amplitudes against the mean Cp and Ct/10 values for the same wave condition are presented for two different wave amplitudes tested. As can be seen in the tables, the amplitudes of both Cp and Ct/10 increased with increasing wave amplitude and decreasing wave frequency. Significant fluctuation can be observed with all three turbines, even more than 50% in Cp and a maximum of 30% in Ct/10. Sin2 turbine generally showed higher level of fluctuation while Sin8 turbine showing the lowest fluctuation. However the differences in the fluctuations amongst the models were limited to small values.

Table 9 Percentage of Cp and Ct/10 fluctuation in regular wave test at wave amplitude=0.05m

Encounter wave frequency	Percentage of Ct/10 fluctuation			Percentage of Cp fluctuation		
(Hz)	Ref	Sin2	Sin8	Ref	Sin2	Sin8
1.54952	2.2%	2.6%	2.1%	5.0%	5.4%	4.5%
1.34957	3.0%	3.5%	2.9%	6.3%	7.1%	6.0%
1.09965	4.8%	4.9%	4.6%	10.1%	10.4%	9.6%
0.89971	7.2%	7.7%	7.0%	15.2%	15.5%	14.3%
0.69978	7.9%	8.3%	7.8%	16.1%	16.4%	16.0%
0.54982	11.9%	12.6%	11.6%	24.5%	25.0%	23.7%
0.39987	13.9%	14.7%	14.0%	28.0%	28.8%	28.2%

Table 10 Percentage of Cp and Ct/10 fluctuation in regular wave test at wave amplitude=0.1m

Encounter wave frequency	Percentage of Ct/10 fluctuation			Percentage of Cp fluctuation		
(Hz)	Ref	Sin2	Sin8	Ref	Sin2	Sin8
1.54923	3.8%	4.0%	4.0%	8.4%	8.2%	8.3%
1.29958	6.6%	7.0%	6.4%	13.5%	14.1%	13.1%
1.09965	10.5%	10.9%	10.1%	21.7%	22.3%	20.9%
0.89971	14.7%	15.5%	14.2%	29.9%	30.8%	28.9%
0.69978	16.4%	17.3%	15.9%	33.0%	34.0%	31.4%
0.54982	23.6%	25.0%	23.0%	47.3%	48.5%	45.9%
0.39987	28.6%	30.0%	27.9%	56.9%	58.2%	55.4%

In Figure 17 the torque and thrust amplitudes of the three turbines were compared against each other over the encounter frequency range tested. As shown in this figure the amplitudes of the torque and thrust of Sin8 turbine were generally lower than those of the other two turbines. This was more obvious in the thrust while the torque of the Sin8 turbine were similar to the reference turbine. A maximum of 4% lower thrust can be achieved with the Sin8 turbine compared to the Ref turbine in the most extreme condition (Wave Amplitude=0.1, Encounter Wave Frequency=0.39987Hz).

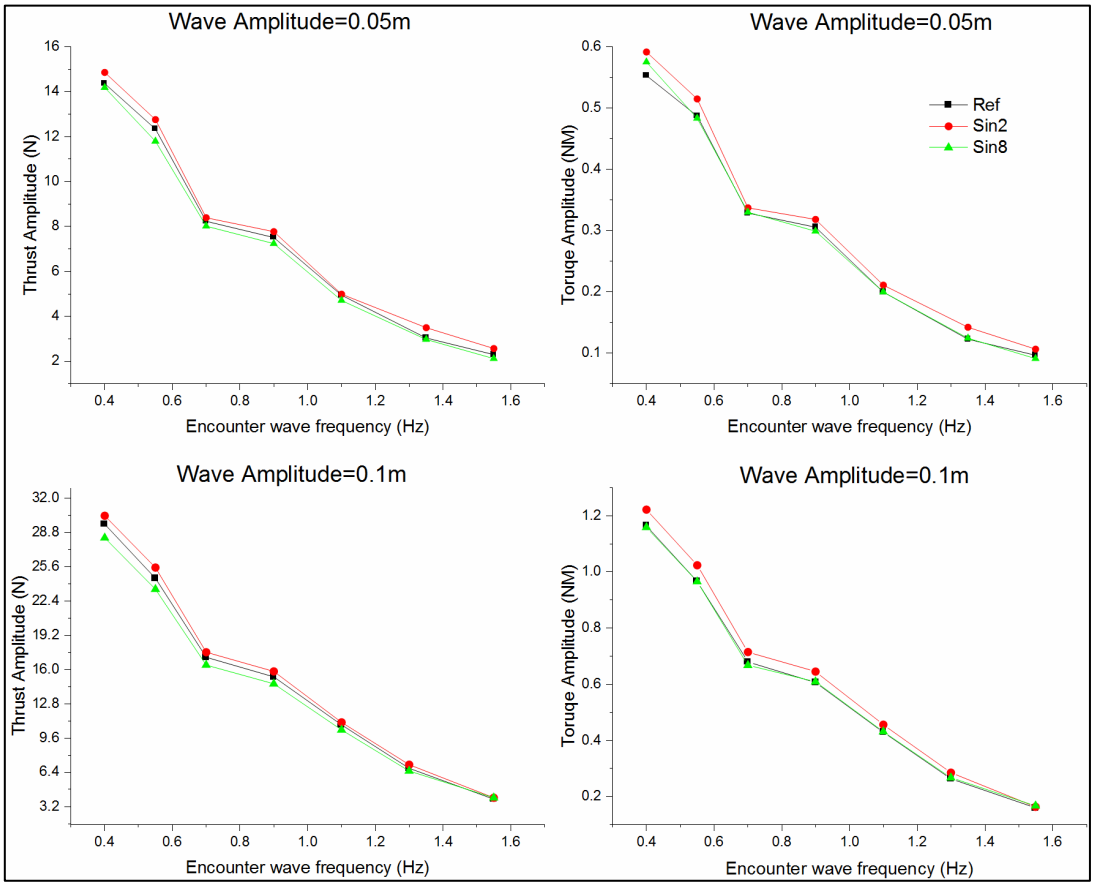

Figure 17 Amplitudes of torque and thrust in regular waves

4.4 Wave-current interaction tests in irregular wave tests

Having completed the performance tests in regular waves, the Ref turbine and Sin8 turbine were tested in irregular head waves which were generated based on the earlier described JONSWAP wave spectra. Figure 18 shows a typical time history of the wave profile generated in the tank for Hs= 0.15m; Tp=1.581s. The wave calibration against the encounter wave frequency is shown in Figure 19. These tests were conducted with the slower carriage speed (V= 0.785 m/s) and single turbine speed, N=150RPM to reflect the full-scale conditions as prescribed in Table 5.

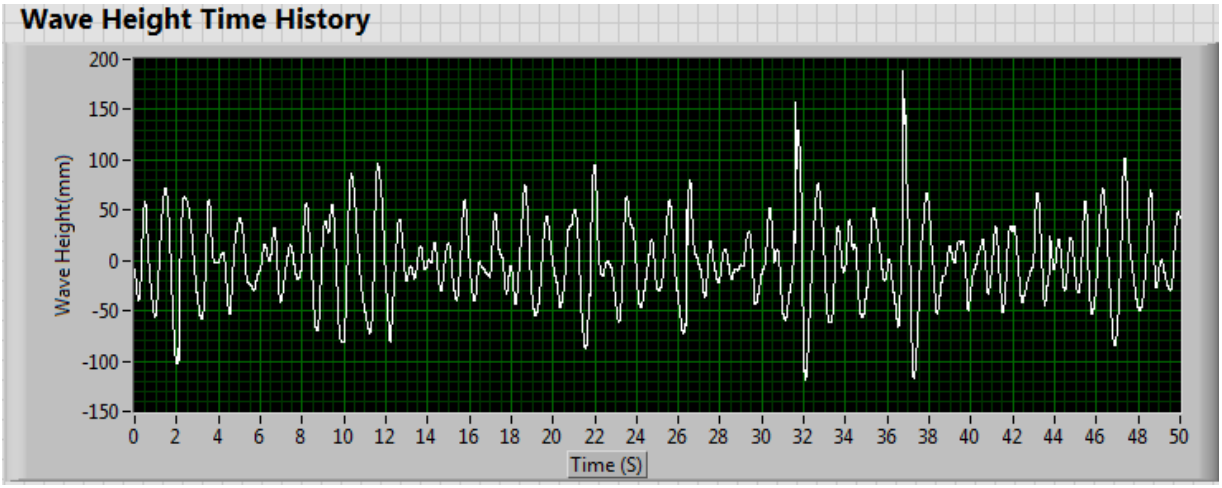

Figure 18 Sample of JONSWAP wave profile (Hs=0.15m, Tp=1.581s)

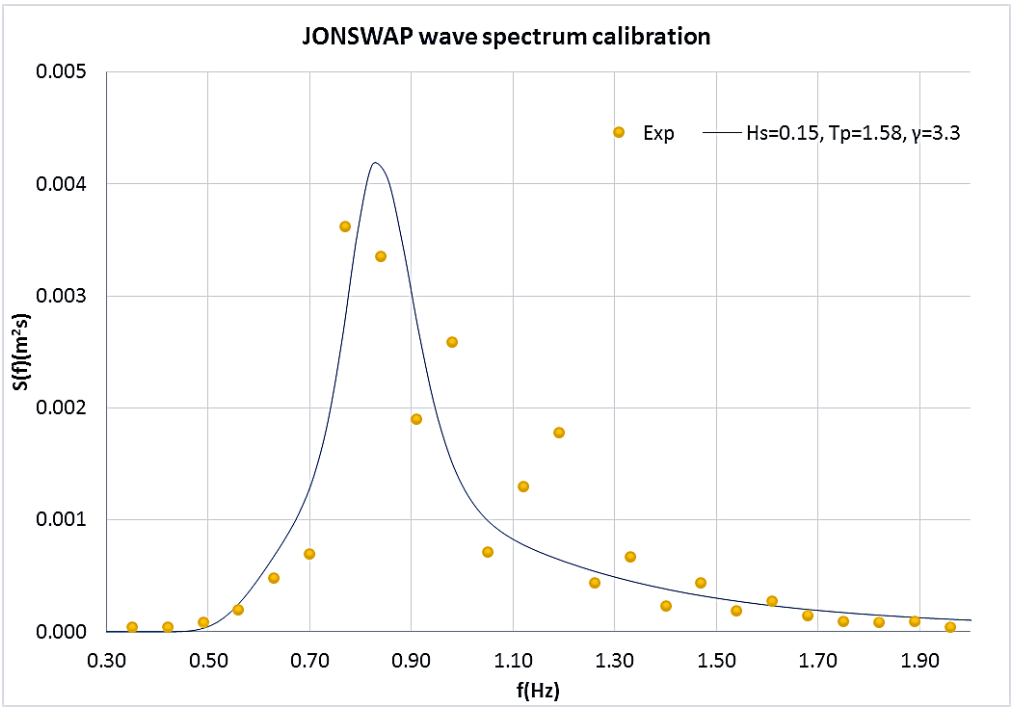

Figure 19 Wave spectrum calibration against encounter wave frequencies (Hs=0.15m, Tp=1.581s)

As previously in the regular wave test, Figure 20 presents the full time history records and peak amplitude FFT analyses of the wave profiles as well as the torque and thrust responses of the Ref turbine for test condition of Hs=150mm; Tp=1.581s, N=150RPM and V=0.785m/s. A closer look at the FFT analyses indicates that apart from the major torque and thrust peak around 0.833 Hz, which corresponds to the encounter frequency for the maximum energy in the wave spectrum (at Tp= 1.581s), there is another local peak at 2.5Hz which corresponds to the shaft rate (150 rpm).

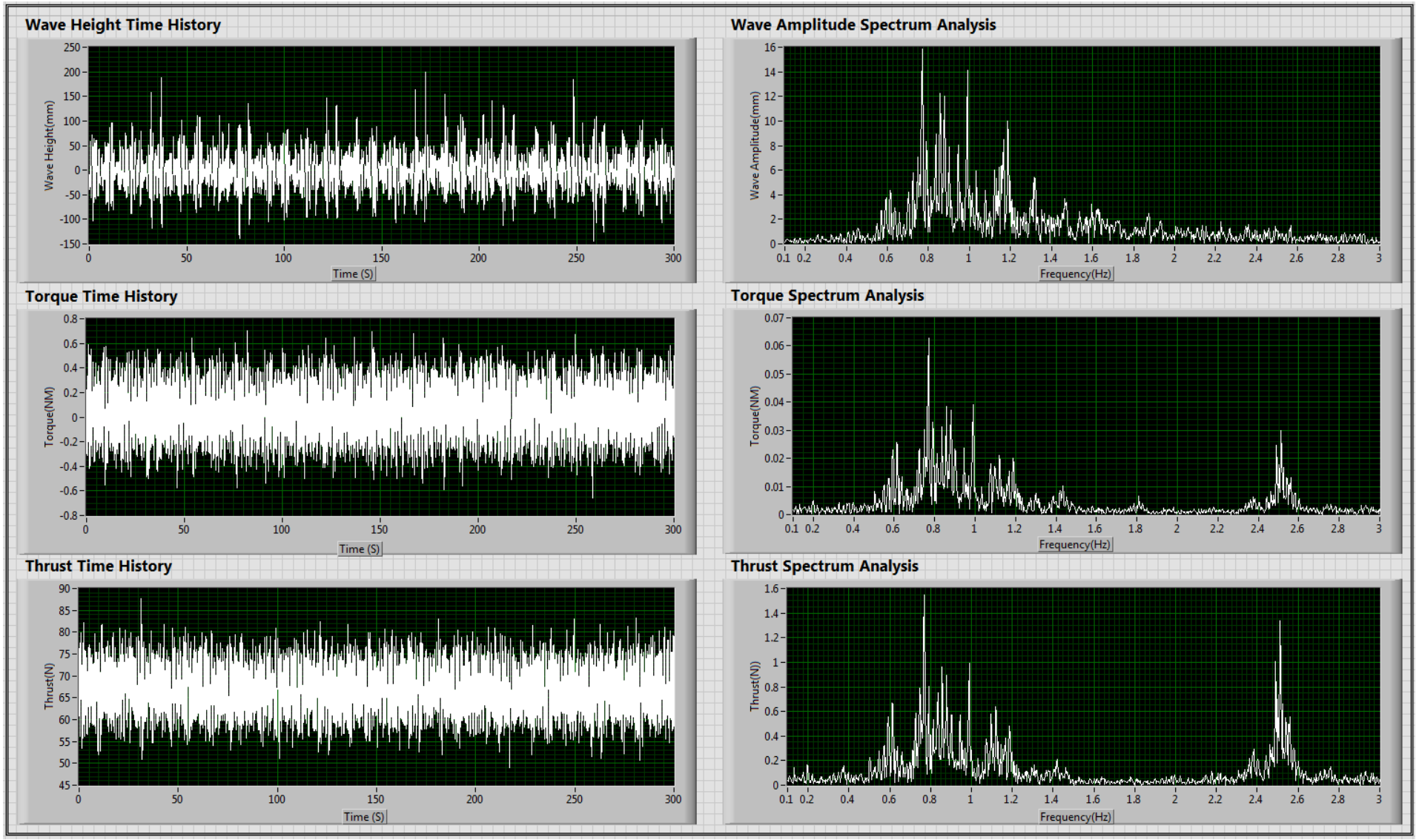

390

391 Figure 20 Time history and FFT analysis for the irregular wave test (Hs=150mm; Tp=1.581s, N=150RPM and V=0.785m/s)

4.4.1 Effect of irregular wave action on the performance of turbines

The analysis was first conducted about the time averaged performance to identify the wave effect on the power generation. The time averaged performance normalized against itself in the calm water has been presented in Table 11.

Table 11 Normalized time average Cp and Ct/10 in irregular waves (JONSWAP)

JONSWAP Hs	JONSWAP Tp	Normalized Averaged Ct/10		Normalized Averaged Cp	
(m)	(s)	Ref	Sin8	Ref	Sin8
0.15	1.581	1.0157	0.9959	1.0512	1.0156
0.25	2.214	1.0144	0.9963	1.1039	1.0469
0.3125	2.372	1.0148	1.0012	1.1320	1.0755
Calm water		1	1	1	1

As it can be easily noticed, the variation on the averaged Ct/10 is very limited (within 2%), with Sin8 even smaller and limited within 1%. On the other hand, the averaged Cp can be improved by the irregular waves, however this might also because of the wave generated turbulence. These phenomena can also be seen in the regular wave test. The Ref turbine can be improved maximum 13.2% under the condition "Hs=0.3125m and Tp=2.372s", but the baseline Cp is only 30% in the calm water at this condition (150RPM) limited by the Reynolds effect while 35.6% for the Sin8. With the increasing Reynolds number as in the full-scale conditions, this kind of enhancement might not exist. But because the variation for the Sin8 turbine caused by the wave effect was very limited compared to the Ref turbine, a more stable power generation performance of Sin8 can be expected.

4.4.2 Effect of irregular wave action on the performance fluctuations of turbines

In order to clarify the wave action on the force fluctuations, the significant values (1/3) of torque and thrust were obtained through the FFT analysis. The results were presented in Table 12.

Table 12 Percentage of significant values of thrust and torque fluctuation in irregular waves (JONSWAP)

JONSWAP Hs	JONSWAP Tp	Percentage of significant thrust fluctuation (1/3)		Percentage of significant torque fluctuation (1/3)	
(m)	(s)	Ref	Sin8	Ref	Sin8
0.15	1.581	35.69%	36.16%	80.66%	76.73%
0.25	2.214	66.60%	71.01%	148.77%	143.32%
0.3125	2.372	80.06%	80.04%	174.62%	159.12%

The result in Table 12 has indicated severe force fluctuations in both torque and thrust. In terms of the torque, the fluctuation of the Sin8 turbine was smaller compared to the Ref turbine especially under the 100-year conditions (Hs=0.3125mm, Tp=2.372s), which indicated around 10% less. However for the thrust, Sin8 showed slight higher value under the 1-year and 10-year conditions (Hs=0.15m, Tp=1.581s and Hs=0. 25mm, Tp=2.214s), but similar level of fluctuation can be observed under the 100-year conditions.

5 Response Amplitude Operator (RAO) for turbine performance

During the analysis of the wave effect on the turbine performance it has been prompted to the Author that there has not been any recommendation or discussion how to define the Response Amplitude Operators (RAO) or the Transfer Functions for the performance of a tidal turbine. Yet, these definitions have been thoroughly investigated and used in the ship motion context as such the ship can be regarded as a linear system and input to the system is the ocean waves and output from the system is being the motion responses. However whether the turbine system can still be regarded as a linear system, as shown in Figure 21, to predict the response as torque or thrust in waves is yet to be concluded (Barltrop et al., 2006, de Jesus Henriques et al., 2014, Tatum et al., 2016). In order to quantify the RAO for the tidal turbine system, the following equation was formulated as below Equation 7.

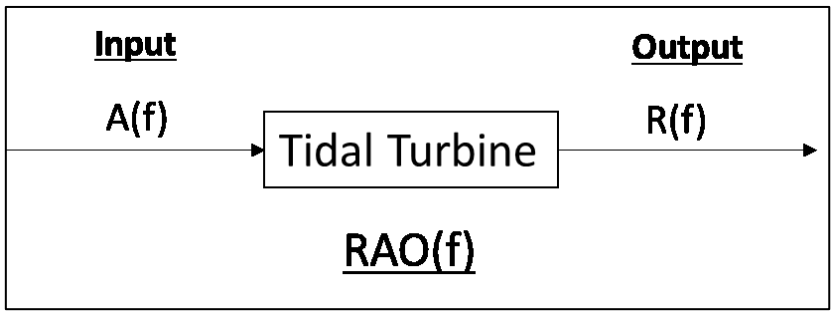

Figure 21 Linear turbine response to the wave action

$$RAO(f) = \frac{R(f)}{A(f)} \qquad \text{Equation 7}$$

where RAO(f) is the response amplitude operators regarding to different wave frequencies, f; R(f) is the response amplitude spectrum of the turbine system; A(f) here is the wave amplitude spectrum. Subscript Q and T will be used to specify the torque or the thrust, respectively.

5.1 RAO in regular waves

In order to investigate the above problem, the Ref turbine is chosen. The RAO analysis for the torque and thrust of this turbine in regular waves is shown in Figure 22. As shown in the figure, the response of the torque and thrust is strongly linear to the wave amplitude, as the curves of $RAO_Q(f)$ and $RAO_T(f)$ with two different wave amplitudes almost overlap each other. Therefore the response of the tidal turbine's performance to the wave actions can be concluded similar to the ship response to the wave actions based on this study.

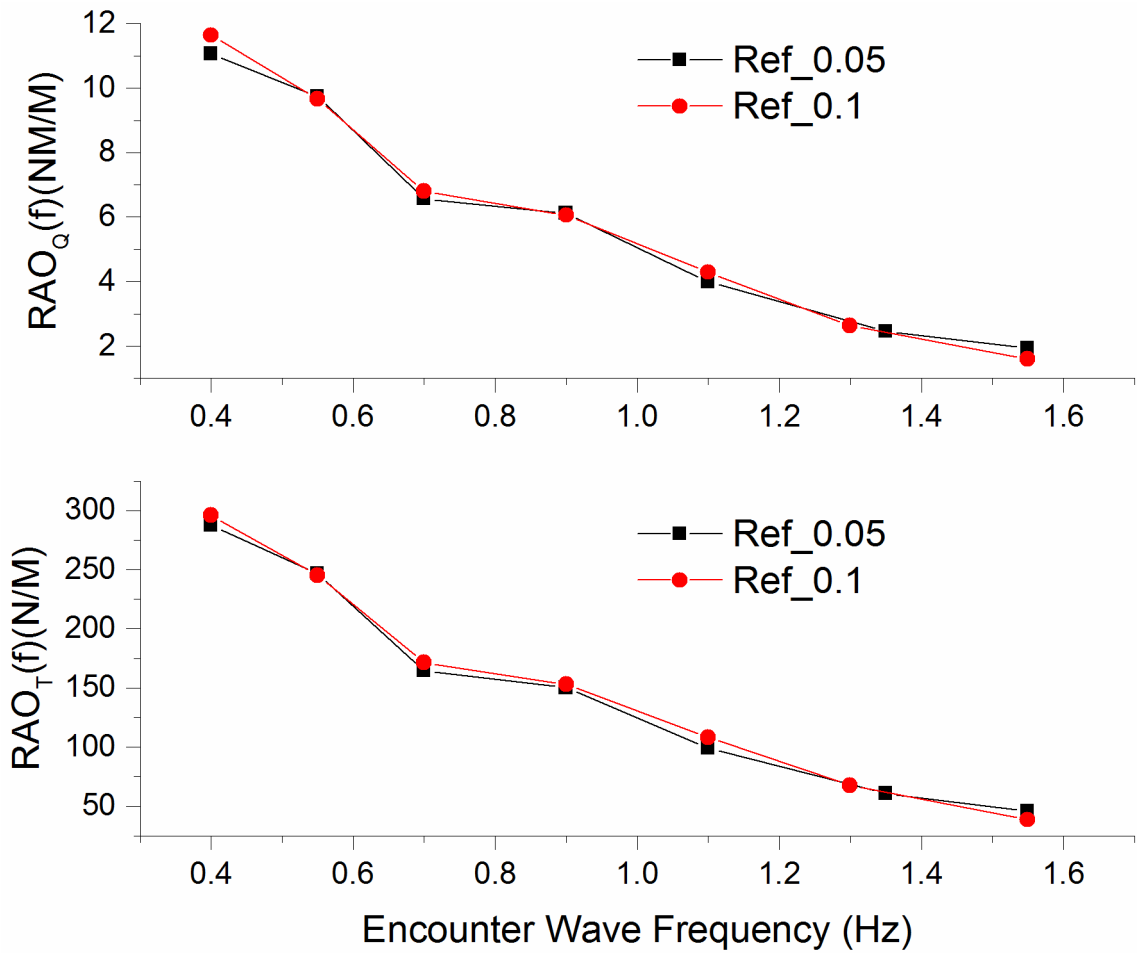

Figure 22 RAOs of the reference turbine in regular waves with 250RPM

The comparisons of RAO in thrust and torque for the three turbines are presented in Figure 25 and Figure 26, respectively, for two different wave heights. In the top right corners of these figures a closer look for the thrust and torque for 0.1m wave amplitude is also included for the sake of easier comparison. From these figures it can be noticed that the Sin8 turbine displayed the lowest RAOs in both torque and thrust while the Sin2 turbine showed the highest.

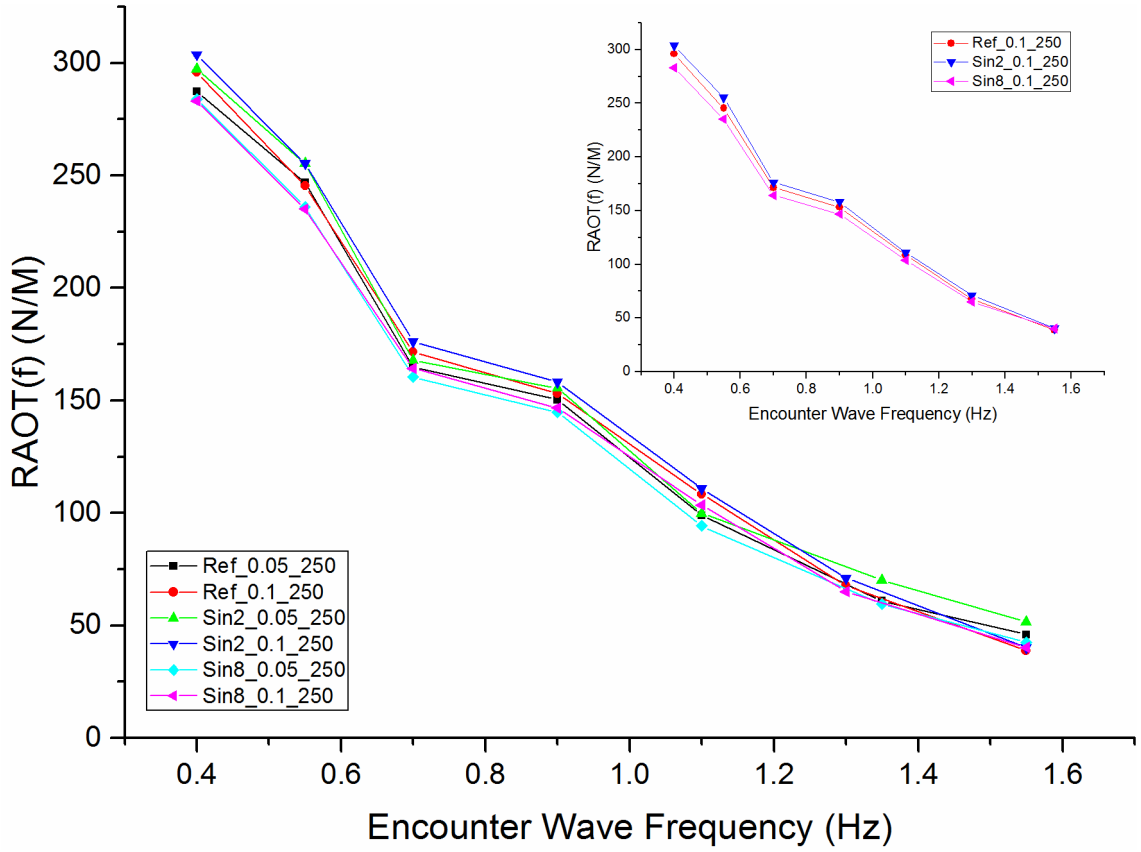

452
453

Figure 23 Comparison of thrust RAO in the regular waves with 250RPM

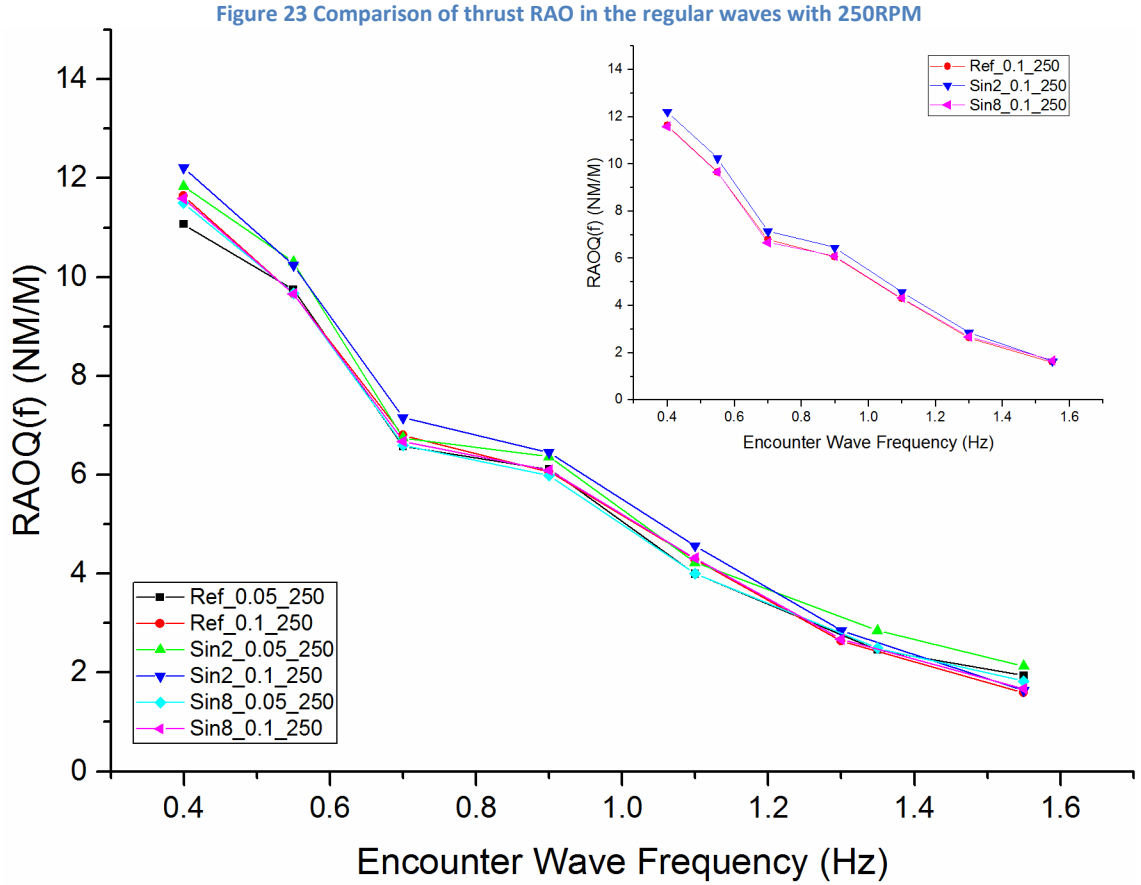

454
455

Figure 24 Comparison of torque RAO in regular waves with 250RPM

5.2 RAO in irregular waves

According to the principle of superposition, irregular waves can be described as a linear superposition of infinite number of simple, regular harmonic wave components. In this sense, the RAO(f) can also be derived from the response spectrum obtained in the irregular wave test. If the linear assumption applied to the turbine system, the RAO(f) measured in regular wave tests and derived from the irregular wave tests should agree with each other.

Therefore, a check on this assumption was conducted and results are shown in Figure 25 where all the tests were repeated with the same carriage speed (0.785m/s) and same RPM (150RPM) for the Refs turbine. In these figures, the lines correspond to the RAOs in regular waves while the dots correspond to the RAO derived from the motion response spectra. For the irregular wave tests, three different JONSWAP wave spectra were used. As it can be seen from these figures the RAO(f)s derived from these tests over majority of the data show close correlations which further validate the hypotheses of the principles of superposition and linear response as applied on the tidal turbine.

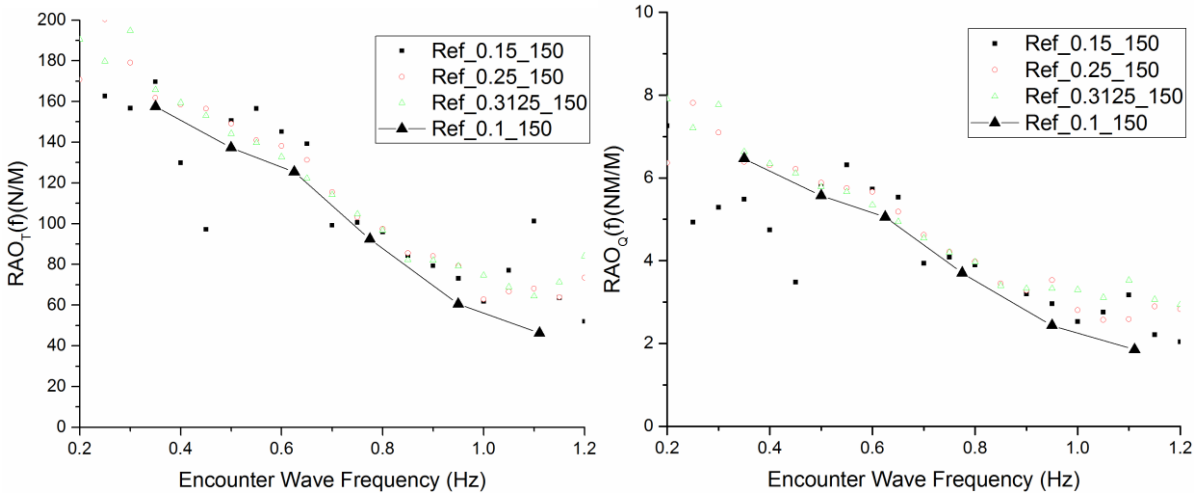

Figure 25 RAO(f) of thrust (left) and torque(right) derived from regular and irregular wave test with 150RPM

5.3 Critical speed correction

However, a closer look into the details of the test results for the derived RAO(f)s with different towing speeds and hence different RPM have significant difference. As it is shown in Figure 26, in spite of the same TSR (4), wave height (0.1m) and encounter frequencies, the RAO(f)s achieved in 1.309m/s and 250RPM are much higher than the result in 0.785m/s and 150RPM. This indicates the effect of free surface (i.e. Fn number) on the results raising the question of what is the RAOs for tidal turbine models under different current speeds, which is commonly experienced in the full-scale when the turbine is operating under various current speeds.

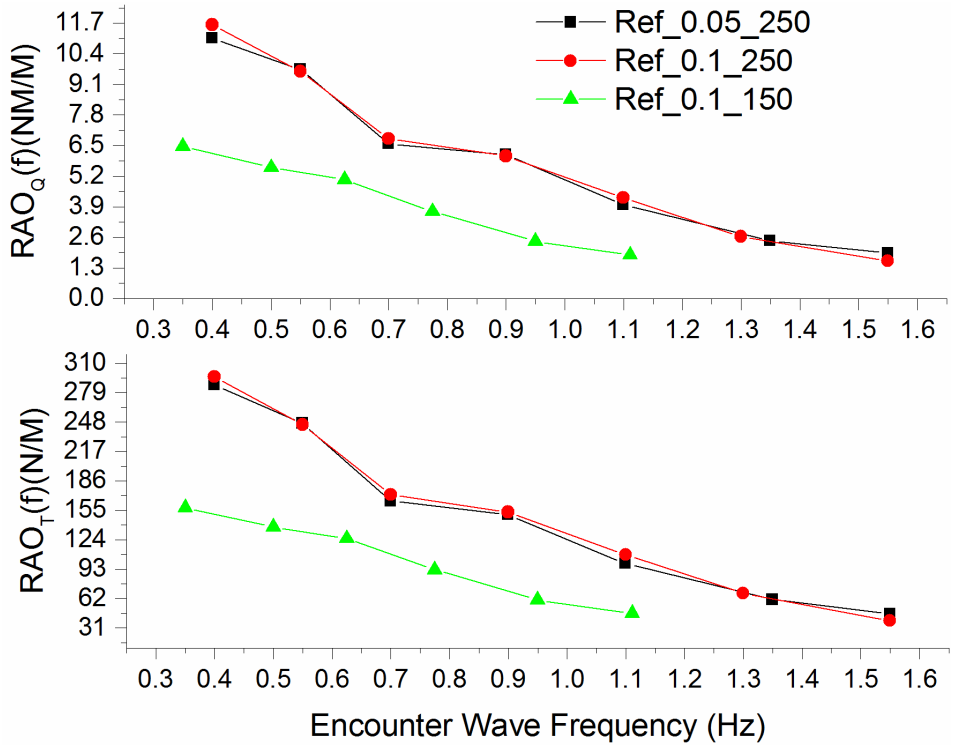

481

482 **Figure 26 RAO(f) of torque (top) and thrust(bottom) tested in different towing speeds**

483 As it has been commonly acknowledged in the wave theory, by ignoring the effect of wave
484 diffraction, the wave action can be simplified and assumed to be mainly causing the cyclic
485 velocity fluctuation at certain level of water depth. Based on this assumption the thrust (T)
486 and torque (Q) of turbine model can be expressed by the thrust and torque coefficients, C_T
487 and C_Q, as follows:

$$T = C_T * \frac{1}{2}\rho A_T V^2 \qquad \text{Equation 8}$$

$$Q = C_Q * \frac{1}{2}\rho A_T V^2 R \qquad \text{Equation 9}$$

488 If the above assumed cyclic velocity fluctuation in the axial direction has an amplitude of ΔV
489 while C_T is assumed to be remained the same, the thrust would fluctuate with the amplitude
490 of ΔT as implied in Equation 10.

$$\Delta T = C_T * \frac{1}{2}\rho A_T[(V + \Delta V)^2 - V^2] \qquad \text{Equation 10}$$

491 Likewise, the above assumption can be made for the torque coefficients as well. Using
492 Equation 8 and Equation 10, the velocity fluctuation can be reversely derived as shown in
493 Equation 11.

$$\Delta V = \mathrm{V} * \left(\sqrt{\left(\frac{\Delta T}{T} + 1 \right)} - 1 \right)$$ Equation 11

The predicted results of ΔV based on Equation 11 for two sets of regular wave test data with two different carriage speeds but at the same wave height are shown in Figure 27. As it can be seen in this figure the simplified correction made for the effect of waves can justify the fact that the main effect of the waves on the turbine performance can be expressed by the contribution in the current speed due to the longitudinal component of the wave particle velocity. This is of course very much dependant on the depth of submergence of the turbine since the effect will be more significant (due to e.g. diffraction etc) and complex as the turbine gets closer to the free surface.

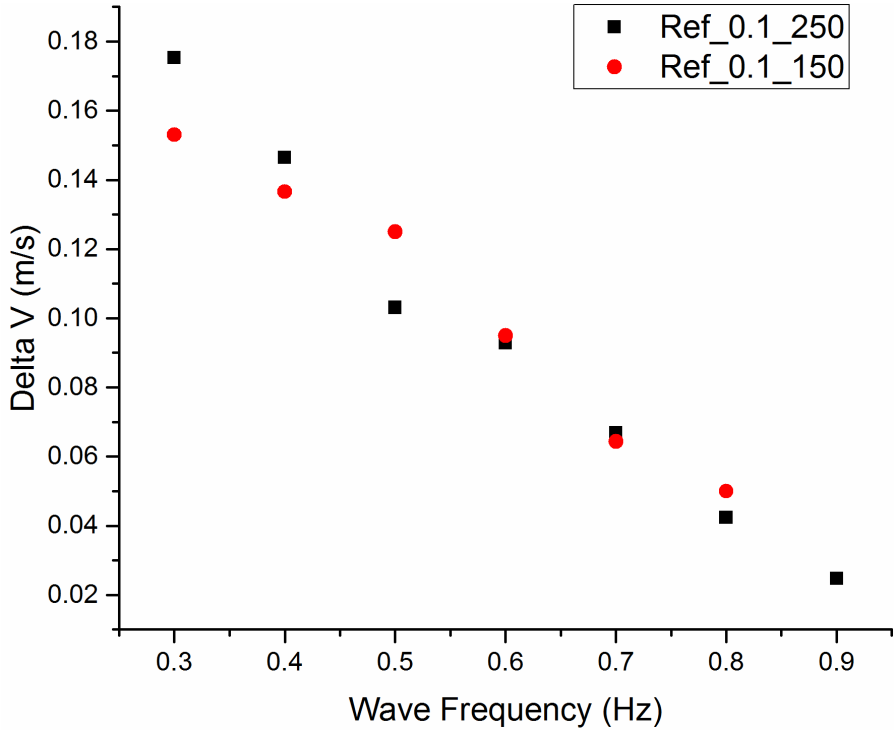

Figure 27 ΔV against the wave frequency as calculated based on two regular wave test data with two different carriage speeds

The above simplified theory has already been applied to calculate the response amplitude caused by the different wave spectrum combined with varied current speeds (Barltrop et al., 2006). In fact Barltrop *et al.* modelled the effect of the orbital wave velocities on the blade forces of a tidal turbine by using a Blade Element Momentum (BEM) theory and achieved close agreement between the predictions and experimental results in the regular waves. However this study has further elaborated the wave action on the tidal turbines.

6 Concluding remarks

Based on the analysed results of the experimental performance tests in waves which were conducted in the KHL with the three model turbines, the following concluding remarks can be reached:

1. The Reynolds number range experienced in the towing tank test was significantly lower than the range in the cavitation tunnel tests, which led to a disparity between the magnitudes of the performance results obtained from the two different facilities. However, the models with the leading-edge tubercles appeared to be less sensitive to the change in the Reynolds numbers compared to the reference turbine. This can be attributed to the potential early transition of the turbulent flow on the turbine blades with the tubercles.

2. Relative comparison of the open water performance of the three turbines tested in calm water in the KHL has further confirmed the main findings of the cavitation tunnel tests where the benefits of leading-edge tubercles have been found to be improving the performance in the low TSRs without interfering the maximum efficiency.

3. The effect of waves on the averaged magnitude of the Cp and Ct/10 coefficients of the three turbines was not as significant as on the fluctuation amplitudes of the same coefficients. Amongst the three turbines, the lowest fluctuation was experienced with the Sin8 turbine while generating the highest power.

4. The RAOs for the torque and thrust data based on the regular wave tests displayed a reasonably linear relationship with the wave height under the same current speed. The Sin8 turbine presented the lowest RAOs over the range of frequencies tested in both torque and thrust while the Sin2 turbine displayed the highest.

5. A further check on the RAOs derived from the response spectra of the irregular wave tests displayed close correlations with the RAOs which were obtained from the regular wave tests. This has further supported the applicability of the superposition principles of the regular wave RAOs for different frequency range to obtain the responses in irregular waves for the prediction of tidal turbine performance.

6. The fluctuating effect of the waves on the performance of a turbine can be included in a simplified manner with a correction in the current speed through the longitudinal component of the orbital wave velocity.

In conclusion, the leading-edge undulated/tubercled tidal turbines have been further investigated in a towing tank under the combination of wave and current actions. It has been confirmed that wave action does not affect the efficiency performance of the turbine but can cause significant force fluctuations which will pose threat to the structures and the generator. Given the benefits of the leading-edge undulated tidal turbines, the initiation of full-scale prototyping has been raised and planned for the future.

Acknowledgement

This research is funded by the School of Marine Science and Technology, Newcastle University and the China Scholarship Council. The financial support obtained from both establishments is gratefully acknowledged. The Authors would also like to thank all the team members in the Kelvin Hydrodynamic Lab for their help in testing and sharing their knowledge.

Reference

BARLTROP, N., VARYANI, K. S., GRANT, A., CLELLAND, D. & PHAM, X. 2006. Wave-current interactions in marine current turbines. *Proceedings of the Institution of Mechanical Engineers, Part M: Journal of Engineering for the Maritime Environment,* 220**,** 195-203.

BOLZON, M. D., KELSO, R. M. & ARJOMANDI, M. 2016. Tubercles and Their Applications. *Journal of Aerospace Engineering,* 29**,** 04015013.

CORSINI, A., DELIBRA, G. & SHEARD, A. G. 2013. On the Role of Leading-Edge Bumps in the Control of Stall Onset in Axial Fan Blades. *Journal of Fluids Engineering-Transactions of the Asme,* 135**,** 081104-081104.

DE JESUS HENRIQUES, T. A., TEDDS, S. C., BOTSARI, A., NAJAFIAN, G., HEDGES, T. S., SUTCLIFFE, C. J., OWEN, I. & POOLE, R. J. 2014. The effects of wave–current interaction on the performance of a model horizontal axis tidal turbine. *International Journal of Marine Energy,* 8**,** 17-35.

FISH, F. E. & BATTLE, J. M. 1996. Hydrodynamic design of the humpback whale flipper. *Journal of Morphology,* 225:51-60.

FISH, F. E., WEBER, P. W., MURRAY, M. M. & HOWLE, L. E. 2011. The tubercles on humpback whales' flippers: application of bio-inspired technology. *Integr Comp Biol,* 51**,** 203-13.

HOWLE, L. E. 2009. Whalepower wenvor blade. Bellequant Engineering, PLLC.

574 IBRAHIM, I. H. & NEW, T. H. 2015. Tubercle modifications in marine propeller blades. *10th*
575 *Pacific Symposium on Flow Visualization and Image Processing.* Naples, Italy.

576 MIKLOSOVIC, D. S., MURRAY, M. M. & HOWLE, L. E. 2007. Experimental evaluation of
577 sinusoidal leading edges. *Journal of Aircraft,* 44**,** 1404-1408.

578 MIKLOSOVIC, D. S., MURRAY, M. M., HOWLE, L. E. & FISH, F. E. 2004. Leading-edge tubercles
579 delay stall on humpback whale (Megaptera novaeangliae) flippers. *Physics of Fluids,*
580 16**,** L39-L42.

581 SHI, W. 2017. *Biomimetic improvement of hydrodynamic performance of horizontal axis tidal*
582 *turbines.* PhD, Newcastle University.

583 SHI, W., ATLAR, M., NORMAN, R., AKTAS, B. & TURKMEN, S. 2016a. Numerical optimization
584 and experimental validation for a tidal turbine blade with leading-edge tubercles.
585 *Renewable Energy,* 96**,** 42-55.

586 SHI, W., ATLAR, M., ROSLI, R., AKTAS, B. & NORMAN, R. 2016b. Cavitation observations and
587 noise measurements of horizontal axis tidal turbines with biomimetic blade leading-
588 edge designs. *Ocean Engineering,* 121**,** 143-155.

589 SHI, W., ROSLI, R., ATLAR, M., NORMAN, R., WANG, D. & YANG, W. 2016c. Hydrodynamic
590 performance evaluation of a tidal turbine with leading-edge tubercles. *Ocean*
591 *Engineering,* 117**,** 246-253.

592 SHI, W., WANG, D., ATLAR, M. & SEO, K.-C. 2013. Flow separation impacts on the
593 hydrodynamic performance analysis of a marine current turbine using CFD.
594 *Proceedings of the Institution of Mechanical Engineers, Part A: Journal of Power and*
595 *Energy,* 227(8)**,** 833–846.

596 STANWAY, M. J. 2008. *Hydrodynamic effects of leading-edge tubercles on control surfaces and*
597 *in flapping foil propulsion.* Msc, Massachusetts Institute of Technology.

598 TATUM, S. C., FROST, C. H., ALLMARK, M., O'DOHERTY, D. M., MASON-JONES, A., PRICKETT,
599 P. W., GROSVENOR, R. I., BYRNE, C. B. & O'DOHERTY, T. 2016. Wave–current
600 interaction effects on tidal stream turbine performance and loading characteristics.
601 *International Journal of Marine Energy,* 14**,** 161-179.

602 WANG, D., ATLAR, M. & SAMPSON, R. 2007. An experimental investigation on cavitation,
603 noise, and slipstream characteristics of ocean stream turbines. *Proceedings of the*
604 *Institution of Mechanical Engineers Part a-Journal of Power and Energy,* 221**,** 219-231.

605 WEBER, P. W., HOWLE, L. E. & MURRAY, M. M. 2010. Lift, Drag, and Cavitation Onset On
606 Rudders With Leading-edge Tubercles. *Marine Technology and Sname News,* 47**,** 27-
607 36.

608